January 2015

Marine Boundary Layer Cloud And Drizzle Properties Over ARM Azores Site

Peng Wu

MARINE BOUNDARY LAYER CLOUD AND DRIZZLE PROPERTIES OVER ARM
AZORES SITE

by

Peng Wu
Bachelor of Science, Nanjing University of Information Science and Technology, 2011

A Thesis
Submitted to the Graduate Faculty

of the

University of North Dakota

In partial fulfillment of the requirements

for the degree of

Master of Science

Grand Forks, North Dakota
August
2015

This thesis, submitted by Peng Wu in partial fulfillment of the requirements for the Degree of Master of Science from the University of North Dakota, has been read by the Faculty Advisory Committee under whom the work has been done, and is hereby approved.

_____
Baike Xi

_____
Xiquan Dong
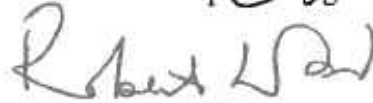
_____
Robert Wood

This thesis is being submitted by the appointed advisory committee as having met all of the requirements of the Graduate School at the University of North Dakota and is hereby approved.
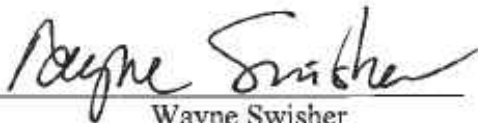
_____
Wayne Swisher
Dean of the Graduate School

_____
July 20, 2015
Date

iii
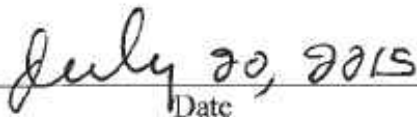
PERMISSION

Title   Marine Boundary Layer Cloud and Drizzle Properties over ARM Azores
               Site

Department   Atmospheric Sciences

Degree   Master of Science

     In presenting this thesis in partial fulfillment of the requirements for a graduate degree from the University of North Dakota, I agree that the library of the University shall make it freely available for inspection. I further agree that permission for extensive copying for scholarly purposes may be granted by the professor why supervised my thesis work or, in her absence, by the chairperson of the department of the dean of the Graduate School. It is understood that any copying or publication or other use of the thesis or part thereof for financial gain shall not be allowed without my written permission. It is also understood that due recognition shall be given to me and to the University of North Dakota in any scholarly use which may be made of any material in my thesis.

Signature:____Peng Wu_____

Date:____07/30/2015_____

TABLE OF CONTENTS

vi

LIST OF FIGURES

LIST OF TABLES

ACKNOWLEDGEMENTS

I would like to thank my advisors, Drs. Baike Xi and Xiquan Dong for providing me the opportunity to work on this research and for their guidance and support. Additionally, I would like to thank my other committee member, Dr. Robert Wood for his comments, suggestions, and expert input into this thesis. In addition, I would like to thank Dr. Timothy Logan and Mr. Ronald Stenz for proof reading the thesis.

My grateful thanks are also extended to the members of my research group, as well as the remaining faculty, staff, and graduate students of the Department of Atmospheric Sciences at the University of North Dakota. Last but not least, I want to thank my family and friends for all of the support they have given me the past two years.

ABSTRACT

In this study, a new method has been developed to retrieve the marine boundary layer (MBL) cloud microphysical properties, which provides a complete diurnal variation of MBL cloud properties for 19-month dataset at the Azores. All nighttime monthly means of cloud liquid water path (*LWP*) exceed their daytime counterparts with an annual mean *LWP* of 140 g m^{-2}, which is ~30.9 g m^{-2} larger than the daytime mean. The seasonal and diurnal variations of cloud *LWC* and optical depth basically follow the variation of *LWP*. There are, however, no significant day-night differences and diurnal variations in cloud-droplet effective radius (r_e) and number concentration (N_t). The corresponding surface measured cloud condensation nuclei (*CCN*) number concentration (N_{CCN}) (at Supersaturation S=0.2%) exhibit a semidiurnal variation. Surface N_{CCN} increases from around sunrise (0300-0600 LT) to late afternoon, which strongly correlates with surface wind speed (r=0.76) from 0300 to 1900 LT. The trend in hourly mean N_t is consistent with N_{CCN} variation from 0000 to 0900 LT, but not for afternoon and evening with an averaged ratio (N_t / N_{CCN}) of 0.35 during the entire study period.

Using potential temperature method and sounding data, all cloud samples were then classified into coupled and decoupled conditions. A schematic diagram is given to demonstrate the coupled and decoupled MBL vertical structures and how they associate with non-drizzle, virga and rain events. Out of a total of 30432 5-min samples (both

daytime and nighttime), 9888 samples can be identified, with 22.2% as coupled and 77.8% as decoupled; 32.7% as non-drizzle and 67.3% as drizzle (47.8% as virga, 19.5% as rain); 40.6% as daytime and 59.4% as nighttime. The averaged thickness of decoupled cloud layer (400 m) is deeper than that of coupled cloud layer (330 m), and its LWP (135.1 g m^{-2}) and r_e (12.7 μm) values are higher than coupled ones (116.4 g m^{-2}, 11.9 μm) too. Conversely, decoupled stratocumuli have lower N_t (80.6 cm^{-3}) and N_{CCN} (180.9 cm^{-3}) than coupled stratocumuli (102.2 cm^{-3}, 210.8 cm^{-3}). The MBL cloud properties under non-drizzle and virga conditions are similar to each other, but significantly different to those of rain.

To further investigate the effect of drizzle on the MBL clouds, drizzle properties below cloud base have been retrieved using lidar and radar observations. For all the cloud and drizzle samples, without considering coupled/decoupled conditions, the drizzle occurrence is 42.6% with a maximum of 55.8% in winter and a minimum of 35.6% in summer. Out of a total of 13092 daytime 5-min samples, 5580 samples can be identified as drizzling cloud, the annual means of drizzle liquid water path (LWP_d), effective radius (r_d) and number concentration (N_d) for the rain (virga) samples are 5.48 (1.29) g m^{-2}, 68.7 (39.5) μm, and 0.14 (0.38) cm^{-3}. The seasonal mean LWP_d values are less than 4% of the MWR-retrieved LWP values. The annual mean differences in cloud-droplet effective radius with and without drizzle are 0.12 and 0.38 μm, respectively, for the virga and rain samples. Therefore, the impact of drizzle on cloud property retrievals is insignificant over ARM Azores site.

CHAPTER I

INTRODUCTION

Stratocumuli cover approximately 23% of the ocean and 12% of the land surface, making them the dominant cloud type by area covered (Warren et al. 1986, 1988; Hahn and Warren 2007; Wood 2012). In particular, marine stratocumulus clouds are ubiquitous over the oceans and play a critical role in boundary layer dynamics and global climate (Klein and Hartmann 1993; Bony and Dufresne 2005). The most extensive marine boundary layer (MBL) clouds occur over the east sides of subtropical oceans, and over mid-latitude oceans under conditions of modest cold air advection during periods of equatorward flow (Klein and Hartmann 1993, Kollias et al. 2007, Wood 2012). These stratocumuli can form under different MBL conditions (either deep or shallow), and a strong temperature inversion at the top of the MBL is favorable for MBL cloud formation (Lilly 1968). These prevailing low-level clouds are a key component in the earth's radiation budget (Randall et al. 1984; Ramanathan et al. 1989). Because most MBL clouds are optically thick clouds (Dong et al. 2014a, b, hereafter D14a, b), they strongly reflect incoming shortwave (SW) radiation (Chen et al. 2000), while weakly affecting outgoing longwave (LW) radiation due to the small temperature difference between the cloud-top and sea surface. This results in a strong net cooling effect on the Earth's surface (Stephens and Greenwald 1991; Hartmann et al. 1992). Longwave cooling at cloud top also generates turbulence from cloud top to surface, this process generates

1

positively buoyant entrained air which contains moisture and cloud condensation nuclei (CCN) that can maintain stratocumulus cover in a well-mixed MBL (Wood 2012).

The climatic importance of the microphysical properties of MBL clouds, particularly the cloud-droplet effective radius (r_e), number concentration (N_t), and liquid water content/path (LWC/LWP), is widely recognized. Slingo (1990) used a climate model to show that a modest relative increase of 15-20% in the cloud fraction, a 15-20% decrease in r_e or a 20-30% increase in LWP could balance the radiative perturbation associated with doubled CO_2 concentrations. Cess et al. (1990) compared 19 GCMs and found a variety of cloud feedback results, ranging from modestly negative to strongly positive because various climate models have different representations of cloud microphysical and radiative properties. An updated comparison by Cess et al. (1996) showed a narrowed difference with most models producing modest cloud feedback which was a result of corrections to cloud optical properties in the models such as improved r_e values. Recent studies, however, indicate little narrowing differences in the cloud feedback spread of the latest model versions (Soden and Vecchi 2011, Dolinar et al. 2015). Therefore, cloud microphysical properties play a key role in cloud feedback and radiative processes in climate models, thus, it is imperative to have more accurate MBL cloud microphysical properties through long-term ground-based observations so that we can improve their representation in climate models.

MBL clouds exhibit strong diurnal modulation largely due to solar insolation and consequently absorption of solar radiation during the daytime in the upper regions of the cloud (Wood 2012). This process suppresses the turbulence generated by cloud top LW cooling, results in weaker circulations during the daytime than at night and a less efficient

coupling of clouds with the surface moisture supply. More moisture and CCN are transported to sustain the development of clouds during night, so the maximum coverage of stratocumulus clouds tends to be during the early morning hours before sunrise. There is also a diurnal cycle of *LWP* that has a maximum magnitude occurring during the early morning hours (Zuidema and Hartmann 1995; Wood et al. 2002a; Bretherton et al. 2004; Zuidema et al. 2005). The amplitude of the diurnal variation in cloud cover and *LWP* can exceed 20% of the mean values (Rozendaal et al. 1995; Wood et al. 2002a) over the eastern subtropical oceans. Microphysical properties, as a result, would also be modulated by the diurnal variation in cloud type, cloud thickness and cloud *LWP*.
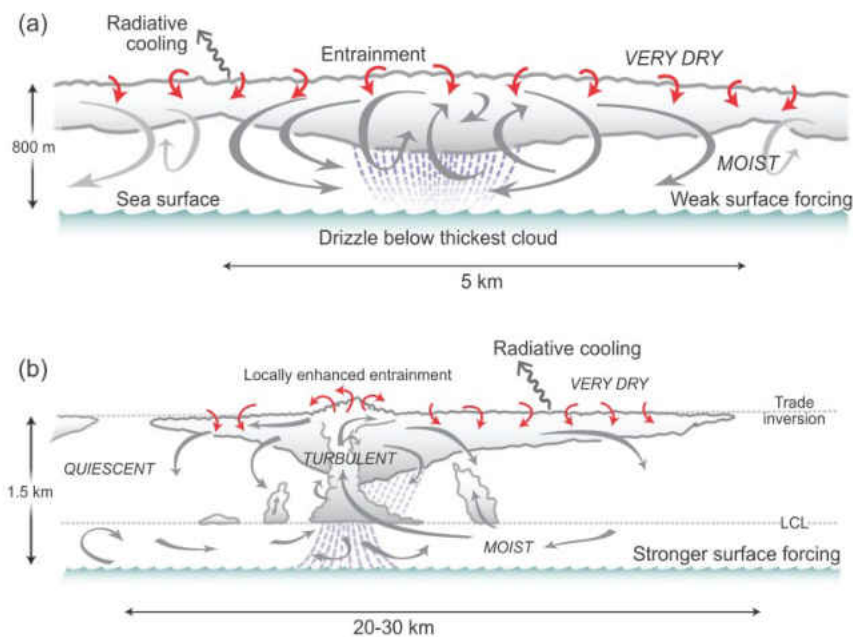
Figure 1. Schematic showing that key processes occur at a stratocumulus-topped boundary layer. The downward arrow for turbulent mixing represents air that is sinking due to radiative cooling at the cloud top, while the upward arrow for turbulent mixing represents rising air caused by the warming of the ocean surface. From Wood (2012).

The vertical structure of the boundary layer can modulate the vertical and horizontal structure of MBL clouds (Lilly 1968; Wood and Bretherton 2004) and consequently, these clouds exhibit different properties under different boundary layer conditions (Dong

et al. 2015, hereafter D15). MBL clouds are turbulently mixed from the top-downward due to negative buoyancy through a combination of LW radiative cooling and evaporative cooling at the cloud top (Wood 2012; Shin and Ha 2009).

The low-level cloud fraction is greatest when the stratocumulus topped boundary layer (STBL) depth (z) is moderately shallow [0.5 km < z < 1.0 km, e.g., Wood and Hartmann (2006)]. These STBLs are often well-mixed with moisture transported from the surface (Fig. 1a) and capped by a strong temperature and humidity inversion just above the cloud layer. Conserved variables such as total water mixing ratio (q_t), and liquid water potential temperature (θ_l) are constant with height in a well-mixed STBL (Nicholls 1984). As the STBL deepens beyond 1 km and the cloud layer depth becomes thick (Fig. 1b), it becomes difficult for LW cooling at the cloud-top to sustain mixing of positively buoyant entrained air over the entire depth of the STBL (Wood 2012). The STBL begins to separate into two layers with the upper layer becoming decoupled from the surface moisture and CCN supply (Wood 2012). In the case of a decoupled STBL, the stratocumulus layer often resides within a well-mixed layer, but the turbulence created by the LW cooling is not strong enough to mix with the sub-cloud boundary layer (Burleyson et al. 2013; Jones et al. 2011; Wood 2012).

MBL clouds frequently produce light precipitation, mostly in the form of drizzle (Austin et al. 1995; Wood 2005a; Leon et al. 2008; Wood 2012). Radar reflectivity thresholds have been widely used to distinguish between non-precipitating and precipitating clouds. For example, Sauvageot and Omar (1987) and Chin et al. (2000) proposed a threshold of -15 dBZ for continental stratocumulus clouds, and Frisch et al. (1995) used -17 dBZ as a threshold to distinguish non-precipitating and precipitating

clouds over North Atlantic. Fox and Illingworth (1997) found that the reflectivity threshold depend on cloud LWC, a specific threshold can detect deferent percentage of drizzle samples in different cloud LWC conditions. Mace and Sassen (2000) found that cloud layers with maximum reflectivity $\geq$ -20 dBZ nearly always contain drizzle for continental clouds over the ARM SGP site. Wang and Geerts (2003), using cloud microphysical data collected from airborne cloud radar off the Oregon coast, demonstrated that the reflectivity thresholds varied from -19 to -16 dBZ for three different cases of marine type clouds and is a function of height within the cloud layer.

When drizzle occurs and falls out of the cloud base, it either evaporates before reaching the surface, which is defined as virga (AMS, 2014), or reaches the surface in the form of rain. Rémillard et al. (2012) identified the virga and rain samples based on the radar reflectivity and whether the lowest range gate of radar echoes reach near the surface (~ 200 m).

The drizzle effect on the STBL is complex (Wood 2012) because it involves the cloud lifetime and evolution (Albrecht 1993; Wood 2000). Drizzle that falls out of the cloud base will deplete cloud water and CCN from the cloud. The evaporation of drizzle below cloud base may drive mesoscale circulations that affect cloud properties (Stevens et al. 1998). Different physical and feedback processes can be induced by virga and rain periods. The evaporation of virga cools the sub-cloud layer and generates turbulence between sub-cloud layer and surface. This turbulence can transport moisture from the surface to the cloud layer to enhance the development of cloud. Wood (2005a) found that the sub-cloud layer with drizzle is generally cooler and wetter than drizzle-free region,

which is a result of evaporation cooling. On the other hand, rain depletes water from the cloud layer to the surface

Zhao et al. (2012) summarized current ARM cloud retrievals. For the treatment of drizzle, some retrieval methods (e.g., COMBRET) classify drizzle from clouds while others just flag the presence of drizzle (e.g., MICROBASE). However, even in COMBRET, they only classify drizzle and do not investigate the impact of drizzle on cloud property retrievals. So far, none of the studies have quantitatively investigated the impact of drizzle on cloud property retrievals.

To investigate MBL cloud properties in various meteorological and aerosol conditions, several field experiments have been conducted: (a) the Atlantic Stratocumulus Transition Experiment (ASTEX) (Albrecht et al. 1995), (b) the First International Satellite Cloud Climatology Project Regional Experiment (FIRE) (Albrecht et al. 1998), (c) the Dynamics and Chemistry of Marine Stratocumulus (DYCOMS) (Stevens et al. 2003), (d) the East Pacific Investigation of Climate (EPIC) (Bretherton et al. 2004), (e) The Marine Stratus/Stratocumulus Experiment (MASE) (Lu et al. 2007) and (f) the Variability of the American Monsoon Systems (VAMOS) Ocean-Cloud-Atmosphere-Land Study Regional Experiment (VOCALS-REx) (Wood et al. 2011, Jones et al. 2011). These field studies have advanced the understanding of stratocumulus cloud development by providing more real time observations of MBL conditions.

These studies, however, are limited to timescales of only a few weeks to a month which is not a long enough period to provide a useful climatology of key MBL cloud properties. In response to this fact, the Atmospheric Radiation Measurement (ARM)

6

mobile facility (AMF) was operational for a 19 months period during the Clouds, Aerosol, and Precipitation in the Marine Boundary Layer (CAP-MBL) campaign, which took place on Graciosa Island in the Azores (Rémillard et al. 2012; Dong et al. 2014a; Wood et al. 2015). It is the first marine stratocumulus field campaign with sophisticated cloud radars on a stable platform that enables the use of the Doppler velocity measurements.

Several recent studies have used these data to improve our understanding of stratocumulus clouds (Rémillard et al. 2012; Logan et al. 2014; D14a, b; Xi et al. 2014; Wood et al. 2015; D15). Rémillard et al. (2012) studied MBL clouds over the Azores using AMF datasets. Liquid precipitation is frequently present (30-40%), mostly in the form of virga. Boundary layer clouds are the most frequently observed cloud type (40-50%), with occurrences peaking during the summer and fall seasons, when the Azores High is dominant. Cumulus clouds are the most common MBL cloud type (20%) with cumulus under stratocumulus layers (10-30%) and single layer stratocumulus (0-10%) following in frequency of occurrence. Rémillard et al. (2012) also found that drizzling stratocumuli have higher LWP and cloud thickness values compared with non-drizzling stratocumuli which is consistent with other studies (Wood 2005a; Zuidema et al. 2005; Serpetzoglou et al. 2008; Kubar et al. 2009).

A complimentary study conducted by D14a produced comprehensive and reliable estimates of seasonal and diurnal variations of marine cloud fraction, MBL cloud macro- and micro- physical properties, and large-scale dynamics. It was found that the single layer low-level cloud fraction was greatest during the summer mainly due to the Azores High. This area of large scale subsidence causes dry weather conditions which are favorable for single-layer MBL clouds. It was also found that seasonal variations of cloud

7

heights and thickness are strongly associated with the synoptic pattern seasonal variations. D14a did provide the diurnal variations of cloud *LWP* and *LWC*. However, they only presented the daytime r_e, N_t, and cloud optical depth (τ), as well as surface measured CCN number concentration (N_{CCN}) and no nighttime retrievals.

D15 chose six coupled and decoupled MBL cloud cases using the potential temperature method and lifting condensation level (LCL) method (Jones et al. 2011; D15). They found that the cloud layer in decoupled MBL is deeper and thicker than in coupledMBL. In addition, the decoupled cloud has higher *LWP* and r_e values but lower N_t and N_{CCN} values than the coupled one. They used linear regression to show that the coupled r_e and N_t strongly depend on surface CCN and have higher correlations with surface CCN than the decoupled cases. D15 also concluded that MBL cloud properties under non-drizzle and virga conditions are similar to each other, but significantly different to those of rain. A schematic diagram (Figure 7 in D15) was shown in D15 to summarize the characteristics of total water content (q_t) and liquid potential temperature (θ_l).

In this study, MBL cloud properties over the Azores will be investigated in a whole diurnal cycle and under different boundary layer conditions. Drizzle below the cloud base will be retrieved and the impact of drizzle below the cloud base on cloud property retrievals will be quantitatively estimated. Section 2 present the datasets and methodology used in this study. Section 3 discusses the results from new retrievals, cloud properties under different boundary layer conditions, drizzle properties and the impact of drizzle to cloud property retrievals. Finally the summary and description of future work is provided in section 4.

8

CHAPTER II

DATA AND METHODOLOGY

Data and Instruments

The datasets used in this study were collected with the Atmospheric Radiation Measurement (ARM) Mobile Facility (AMF) which was deployed near the north shore of Graciosa Island, Azores, from June 2009 through December 2010. Graciosa is a small island (a 60 km^2 area) situated at 39.1°N, 28.0°W, in the Azores archipelago (Fig. 2) at a latitude that straddles the boundary between the subtropics and the mid-latitudes (Wood et al. 2015).
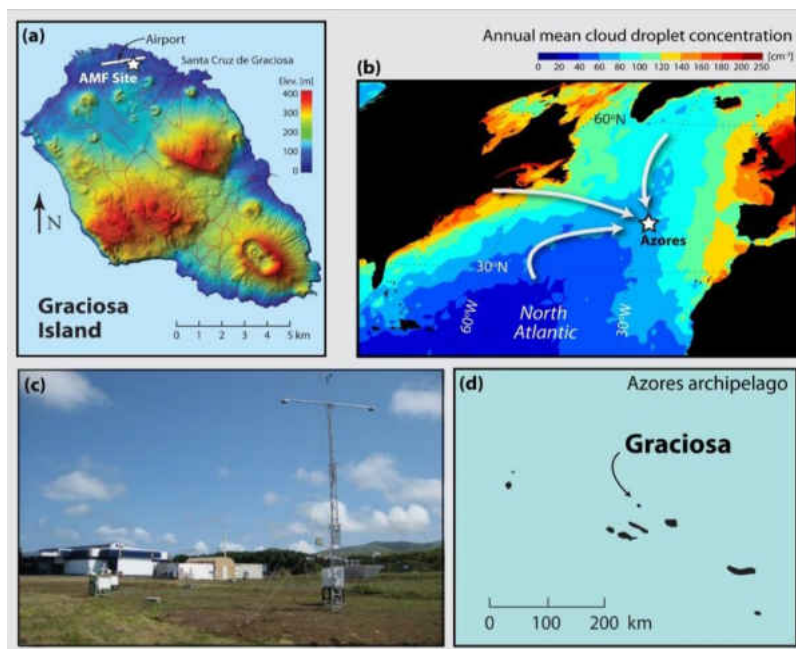
Figure 2. (a) Map of Graciosa Island and the location of the AMF site. (b) Location of the Azores in the North Atlantic. (c) Photograph of the AMF site looking to the SE; (d) Map of the location of Graciosa (and Pico) in the Azores archipelago. From Wood et al. (2015).

Graciosa Island is an ideal location to study MBL clouds over the remote subtropical Northeast Atlantic Ocean (NEA) (Wood 2009, 2015), because it is sufficiently remote and clear of direct continental influence (1300 km from Europe). Island effects on measurements are minimal because winds are predominantly from the north and west (D14a; Wood et al. 2015). The Azores typically experiences relatively clean conditions advected from the central North Atlantic that produce nearly pristine MBL clouds, but periodically experience episodes of polluted air masses advected from Western Europe, North Africa, and North America (Logan et al. 2014; Wood et al. 2015).
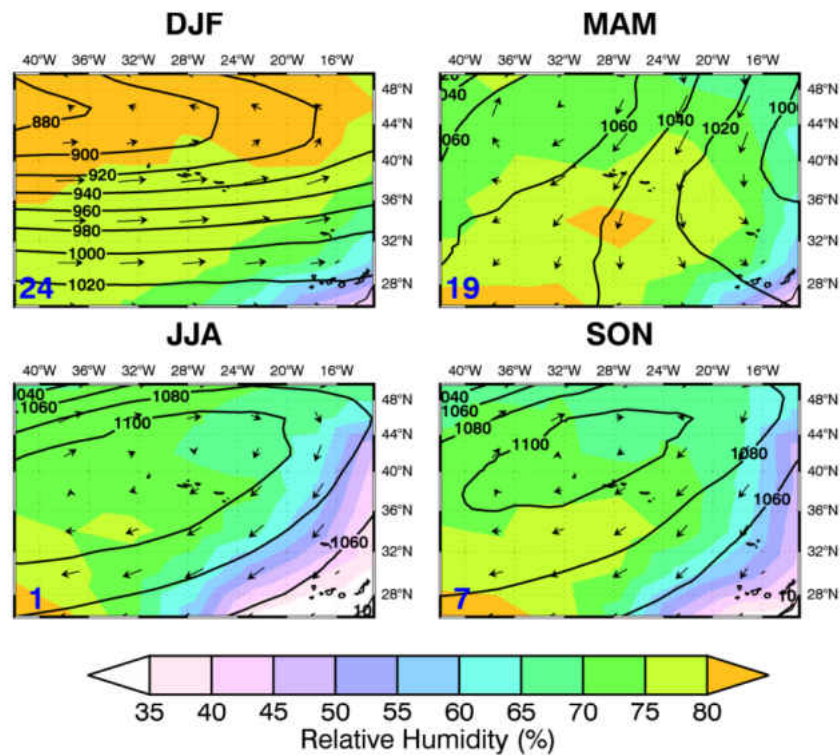
Figure 3. 900 hPa Analysis based on the NASA MERRA reanalysis during the period June 2009-December 2010. The grid box covers a range of latitudes from 26-50°N and longitudes from 42-12°W centered on the ARM Azores site. Shown are 900 hPa geopotential heights, wind vectors, and shaded contours of relative humidity. The four seasons are winter (DJF), Spring (MAM), summer (JJA) and Fall (SON). From D14a.

The Azores is subject to a wide range of different meteorological conditions. From the 900 hPa analysis based on the NASA MERRA reanalysis during the period June 2009-December 2010, as illustrated in Fig. 3, low pressure systems are dominant over the Azores during the winter months which induce anomalous westerly winds that transport moist air masses (RH ~75%-85%) from the north Atlantic to the Azores, producing more multilayered clouds and deep frontal clouds associated with mid-latitude cyclones. During the summer and other seasons, persistent high pressure systems (Azores High) give rise to relatively dry conditions [relative humidity (RH) ~65%-75%] which results in a transition from an overcast stratocumulus regime to a broken trade cumulus regime.

The instrumentation deployed during the CAP-MBL campaign was detailed in Rémillard et al. (2012) and Wood et al. (2015). The primary instruments/observations used in this study to describe cloud and precipitation conditions include a W-band (95-GHz) Doppler radar, a Vaisala ceilometer, a two channel microwave radiometer, balloon-borne sounding system/merged soundings, surface aerosol observing system and a total sky imager. The instruments/observations were placed within a few meters of each other so that their measurements describe the same atmospheric column. Overall, the observations are fairly continuous with significant overlap between the four remote sensors, both spatially and temporally (Rémillard et al. 2012). In the next sub-sections, each instrument/observation is discussed in greater detail.

W-band (95-GHz) Doppler Radar

The W-Band ARM Cloud Radar (WACR) systems are vertically pointing Doppler radars that observe the extent and composition of clouds at 95.04 GHz. Unlike the millimeter wavelength cloud radar (MMCR, 35 Ghz), the WACR does not use pulse

coding and operates in only co-polarization and cross-polarization modes. Millimeter wavelength radars are ideally suited for the study of MBL and high-level clouds (Kollias et al. 2007) owing to its short wavelength (3.15 mm), which is sensitive enough to detect cloud droplets (-50 dBZ at 2 km), while only slightly attenuating when light to moderate drizzle is present. The WACR also provides high temporal and vertical resolutions (around 2 s and 43 m) because it uses a narrow beamwidth (0.19°).

The WACR began operating on the morning of 5 June 2009 and was in operation until the end of December 2010. One major interruption occurred in September 2010, when the radar was down for 23 straight days, due to a hard disk problem. The radar also experienced six non-consecutive additional interruptions of more than an hour (Rémillard et al. 2012). In this study, the reflectivity, Doppler velocity and spectrum width from WACR observations will be used in cloud and drizzle properties retrievals.

Vaisala Ceilometer

The Vaisala Ceilometer (CEIL) is a self-contained, ground-based, active, remote sensing device designed to measure cloud-base height and vertical visibility. The WACR is sensitive to the sixth moment of the cloud particle distribution, while the laser ceilometer are sensitive to the second moment. Consequently, many studies have combined radar and lidar measurements to estimate cloud fraction and boundaries (e.g., D14a and D15). Thus, the bottom of a cloud layer will be taken to be the cloud base heights used in this study. It has a maximum vertical range of 7700 m. It has a vertical resolution of 15 m and temporal resolution of 15 s (Morris 2012; Wood 2015). The CEIL is more accurate at depicting the cloud base height than the WACR, and is more accurate

than the micropulse lidar (MPL) during heavy drizzle because MPL signals are heavily attenuated.

Similar to other instruments, the CEIL also provided nearly continuous measurements during the whole campaign (Rémillard et al. 2012). It only experienced 12 interruptions lasting more than an hour (including three covering more than a day) as well as a small number of shorter interruptions. In this study, the attenuated backscatter coefficient will be used to retrieve drizzle properties below the cloud base using the method proposed by O'Connor et al. (2005). The ratio of radar reflectivity to lidar backscatter is proportional to the forth power of drizzle particle size so potentially can provide an accurate size estimate.

Microwave Radiometer

The Microwave Radiometer (MWR) is used to measure time-series brightness temperatures at the frequencies of 23.8 GHz and 31.4 GHz which are sensitive to water vapor and liquid water, respectively. The temporal resolution of the MWR measurements is around 20 s. The brightness temperatures measured with the MWR are then used to retrieve the atmospheric column integrated water vapor (PWV) and LWP using a statistical method (Liljegren et al. 2001). The root-mean-square (RMS) accuracy of the LWP retrieval is 20 g m^{-2} and 10% for cloud LWP above and below 200 g m^{-2} (Liljegren et al. 2001; Dong et al. 2000).

Balloon-borne Sounding System/Merged Soundings

The balloon-borne sounding system (SONDE) provides *in situ* measurements (vertical profiles) of both the thermodynamic state of the atmosphere and wind speed and direction. SONDEs measure the following parameters as functions of height: pressure

(hPa), temperature (°C), relative humidity (RH%), wind speed (m/s), and wind direction

(degrees). Secondary quantities included in the data stream include: altitude (gpm), dew

point (°C), ascent rate (m/s), latitude of sonde (°N), longitude of sonde (°W),

u-component of wind velocity (m/s), and v-component of wind velocity (m/s). All of

these measurements have a 95.5% confidence level. These radiosondes are launched

regularly at 6 hour intervals (Holdridge et al. 2011). During the AMF deployment, more

than 2200 atmospheric profiles were collected with SONDEs, although no SONDEs were

launched in the last third of October 2009 or from 2 December 2009 through 12 January

2010.

The Merged Sounding (MERGESONDE) value-added product (VAP) uses a

combination of observations from radiosonde soundings, the MWR, surface

meteorological instruments, and the European Centre for Medium-Range Weather

Forecasts (ECMWF) model output with a scaling/interpolation/smoothing scheme in

order to produce profiles of the atmospheric thermodynamic state in 1-min temporal

intervals for and a total of 266 altitude levels (Table 1, Troyan, 2012).

Table 1. The vertical resolution for all MERGESONDE altitude levels.

Altitude Range	Resolution
0-3 km AGL	20 m
3-13 km AGL	50 m
13-16 km AGL	100 m
16-20 km AGL	200 m

Surface Aerosol Observing System

The Aerosol Observing System (AOS) is a suite of *in situ* surface measurements of

aerosol optical and cloud-forming properties. The primary optical measurements are

those of the aerosol scattering and absorption coefficients as a function of particle size and radiation wavelength, and of N_{CCN} measurements as a function of percent super-saturation (Wood, 2015). The N_{CCN} parameter used in this study was calculated using hourly averaged measurements from a Droplet Measurement Technology (DMT) Model 1 optical particle counter at 0.2% supersaturation by the AMF Aerosol Observation System at the Azores (Jefferson et al. 2010).

Total Sky Imager

The total sky imager (TSI) provides time series of hemispheric sky images during daytime. The images were used to confirm the type of drizzle (virga or rain) identified by WACR in daytime. If water spots were present in the image, this sample is classified as rain, otherwise this sample is classified into virga.

Each instrument/observation used in this study has different time resolution from the other, so all data retrieved or collected from each instrument/observation are averaged into five minute intervals in this study. This reduces instrument noise and data size, making each data set more manageable.

Methodology

Cloud Property Retrieval Algorithm

Following the method of Dong and Mace (2003, hereafter DM03), we develop a new method to retrieve the MBL cloud-droplet effective radius profile $r_e(h)$ in this study, which is independent of solar transmission and can be used during both daytime and nighttime, as well as for multi-layered cloud conditions. We derive an empirical relationship between the daytime retrieved $r_e(h)$ and the WACR reflectivity profile from single-layered and overcast MBL clouds and apply this relationship to nighttime retrievals.

Following the criteria described in D14a, a total 1091 hours of daytime and 1445 hours of nighttime single-layered and overcast low clouds, and their corresponding surface CCN measurements, have been selected. Five criteria were established for choosing the conditions under which daytime cloud properties can be estimated: (i) only single-layer and overcast low clouds are present as determined from cloud radar/lidar observations, (ii) Z_{top} < 3 km, (iii) 20 < LWP < 700 gm^{-2}, (iv) cosine of solar zenith angle (μ_0) > 0.1, and (v) 0.08 < solar transmission (γ) < 0.7. The criteria (i)-(iii) for selecting daytime cloudy cases have been used for choosing the nighttime cloudy cases in this study.

The layer-mean cloud-droplet effective radius ($\overline{r_e}$) during the daytime was parameterized as a function of cloud *LWP*, γ, and μ_0 (Dong et al. 1998, hereafter D98) and is given by the following expression:

$$\overline{r_e} = -2.07 + 2.49LWP + 10.25\gamma - 0.25\mu_0 + 20.28LWP\gamma - 3.14LWP\mu_{0,} \qquad (1)$$

where the units of $\overline{r_e}$ and *LWP* are in μm and 100 g m^{-2}, respectively. Following the development DM03 and mathematical derivations, and collecting constant terms, we can infer r_e profile as follows:

$$r_e(h) = \overline{r_e} \left[\frac{\Delta H}{\Delta h} \frac{Z^{1/2}(h)}{\sum\limits_{base}^{top} Z^{1/2}(h)} \right]^{1/3}, \tag{2}$$

where ΔH is cloud thickness (m), and Δh is the radar range gate spacing (43 m in this study). In addition, $r_e(h)$ is proportional to both the $\overline{r_e}$ calculated in (1) and the ratio of the radar reflectivity to the integrated radar reflectivity.

The cloud particle size distribution is assumed a single mode lognormal size distribution

$$Z(h) = 2^6 10^{-12} N_t r_e^6(h) \exp(3\sigma_X^3), \tag{3}$$

where σ_X is the logarithmic width of the size distribution, and the units of $r_e(h), Z(h)$, and N_t are $\mu m, mm^6 m^{-3}$ and cm^{-3}, respectively. Taking the logarithm of both sides of (3) and multiplying by 10 to change $Z(h)$ to $dBZ(h)$, we obtain

$$10\log Z(h) = 10\log[\,2^6 10^{-12} N r_e^6(h)\exp(3\sigma_X^2)], \tag{4}$$

which can be written as

$$dBZ(h) = 10[1.806 - 12 + 0.4343\ln N + 2.606\ln r_e(h) + 1.303\sigma_X^2]. \tag{5}$$

Solving for $r_e(h)$ we obtain the final expression

$$r_e(h) = \frac{\exp(3.912 - 0.5\sigma_X^2)}{N^{0.167}} \exp[0.0384 dBZ(h)] = a\exp[0.0384 dBZ(h)]. \tag{6}$$

The coefficient *a* may not necessarily remain a constant but does depend on the characteristics of the particle size distribution that are driven by such factors as N_{CCN},

updraft velocities, and water vapor supersaturation. Therefore, it is reasonable to assume that the coefficient *a* will depend on different meteorological factors and air masses.
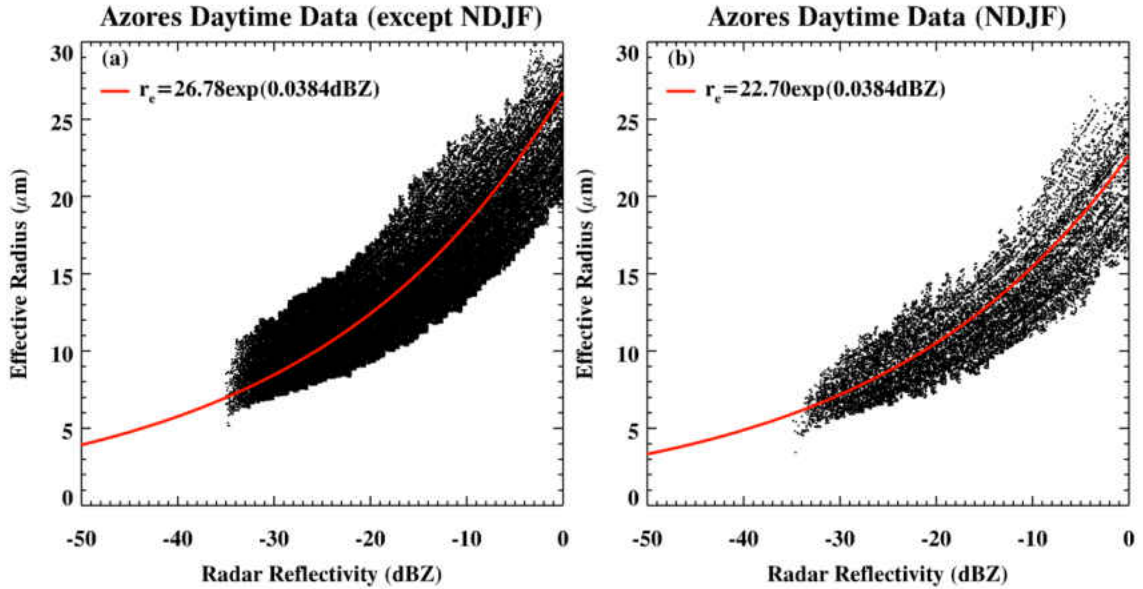
Figure 4. Empirical relationships between the retrieved daytime cloud-droplet effective radius $r_e(h)$ and the W-band ARM Cloud Radar (WACR, 95-GHz) reflectivity from single-layered and overcast MBL clouds during the 19-month period. The points on the scatterplot are derived from (2) while the regression lines are plotted using best-fit values in (a) for all months except for NDJF, a=26.78, and (b) NDJF, a= 22.70 in (6).

As illustrated in Fig 3 and discussed in Section 2, low pressure systems are dominant over the Azores during the winter months which induce anomalous westerly winds that transport moist air masses (RH ~75%-85%) from the north Atlantic to the Azores, producing more multilayered clouds and deep frontal clouds associated with mid-latitude cyclones. During the summer and other seasons, persistent high pressure systems give rise to relatively dry conditions (RH ~65%-75%) and a transition from an overcast stratocumulus regime to a broken trade cumulus regime. Therefore we derive two empirical coefficients between $r_e(h)$ and dBZ(h) corresponding to the winter months (a = 22.7 for November-February) and other months (a = 26.78) during the 19-month period as shown in Fig. 4. Although the method is the same in this study and

DM03, the empirical relationships ($a = 22.7$ from Nov. to Feb. and $a = 26.78$ for other months) in this study and DM03 ($a = 22.0$) are slightly different, which may be attributed to the reasons discussed in the following paragraphs.
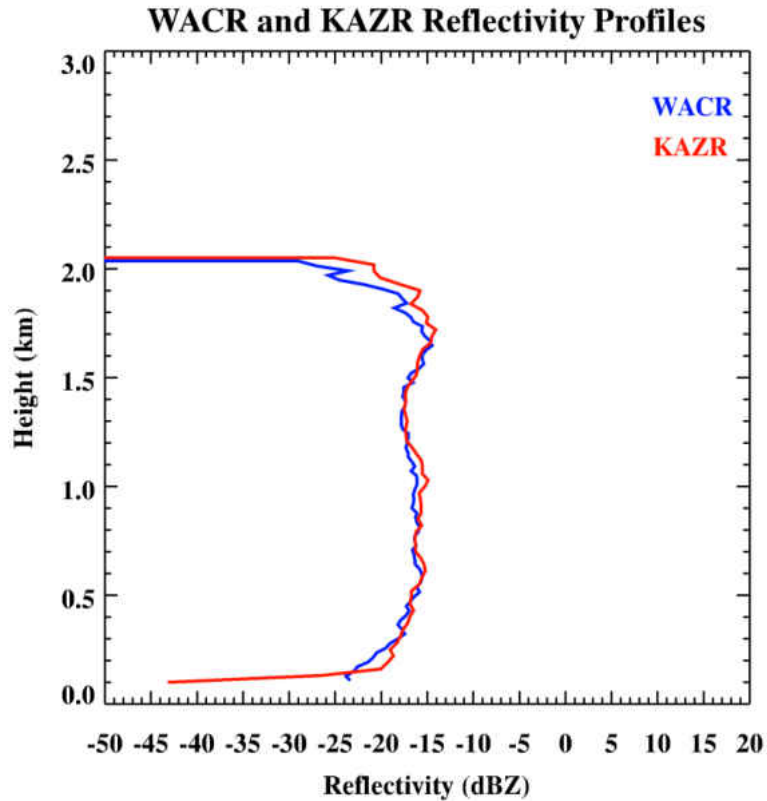
Figure 5. Comparison between W-band (94 GHz) and Ka-band (35 GHz) cloud radar reflectivity profiles from ARM MAGIC field campaign. Blue and red lines represent WACR and KAZR reflectivity profiles on Nov. 13, 2012, respectively.

At first, the cloud radar wavelength is different. The cloud radar at the Azores was 95 GHz while it was 35 GHz at the ARM SGP site. Although we do not compare these two radar reflectivities directly at those two sites, the preliminary comparison during the Marine Atmospheric Radiation Measurement ARM GPCI[1] Investigation of Clouds (MAGIC) field campaign shows that there is no significant difference between the two radar reflectivity measurements (an example is shown in Fig. 5). Second, the low-level

---

[1] GPCI: Global Energy and Water Cycle Experiment (GEWEX) Cloud System Studies (GCSS) Pacific Cross-section Intercomparison

clouds at the Azores represent typical MBL clouds, while they are continental clouds at

the ARM SGP site. Based on the statistical results from previous studies (e.g., Dong et al.

2005 and D14a), the averaged daytime $\overline{r_e}$ values are 8.7 μm and 12.5 μm, respectively,

for typical continental and MBL cloud $\overline{r_e}$ values. Other meteorological factors, such as

vertical velocity, aerosol, synoptic pattern, and water vapor supersaturation level over

these two sites, may also attribute to the difference in parameter a.

The derived empirical relationships can be applied to calculate r_e values for

nighttime and multilayer clouds. The layer-mean cloud-droplet effective radius $\overline{r_e}$ is

linearly averaged $r_e(h)$ from cloud base to cloud top. Once $\overline{r_e}$ is known, we can use the

same method used during the daytime to calculate N_t and τ as follows:

$$N_t = \left[\frac{3LWP}{4\pi\rho_w r_e^3 \Delta Z}\right] \exp(3\sigma_x^2), \tag{7}$$

and

$$\tau = \frac{3Q_{ext}LWP}{4\rho_w r_e}. \tag{8}$$

The logarithmic width σ_x is set to 0.38 (Miles et al. 2000), and the broadband

shortwave extinction efficiency (Q_{ext}) is set to 2.1 for $r_e \sim 14$ μm (Dong et al. 1997).

Since no concurrent in situ data are available for evaluating the nighttime retrievals over

the Azores, the 15-20% uncertainties for r_e and τ, and 30% for N_t estimated from the

daytime aircraft in situ measurements during the March 2000 field campaign at the ARM

Southern Great Plains (SGP, DM03) should be used as reference. Even though the

WACR reflectivity is consistent between day and night, and the potential differences in

meteorological factors between day and night may influence the accuracy of nighttime

retrievals. Therefore, the uncertainties of the nighttime retrievals at the Azores should be

larger than the suggested ones from the ARM SGP site. However, it is difficult to quantitatively estimate to what extent without the aid of aircraft in situ measurements. In order to check whether the results from the empirical relationship are reasonable or not, we compared the layer mean daytime r_e calculated from the relationship with the results from D98, the comparison is shown in Fig. 6. Also shown in Fig. 6 is the nighttime results calculated from (6). In general, the daytime results from D98 and (6) agree with each other except for September 2010 (16th month in Fig. 6). A possible reason is that WACR was down for almost 23 days, due to a hard disk problem (Rémillard et al. 2012; Wood, 2015), thus the result from (6) for this month only used 8 days of data, which was insufficient to represent the cloud properties during the whole month. The nighttime results follow the trend of daytime values except for September 2010. Note that the nighttime r_e are generally larger than that for daytime because the clouds are coupled with surface moisture supply during the nighttime while the clouds in the daytime are decoupled with the surface. This is also consistent with other studies in which they found cloud LWP are higher in nighttime and early morning than in daytime (Zuidema and Hartmann 1995; Wood et al. 2002; Bretherton et al. 2004; Zuidema et al. 2005; D14a).

Figure 6 also suggest that the newly fitted relationship of r_e and reflectivity (Eq. 6) can be used in cloud property retrievals for both daytime and nighttime, since for both time periods, the results are consistent with that from D98.
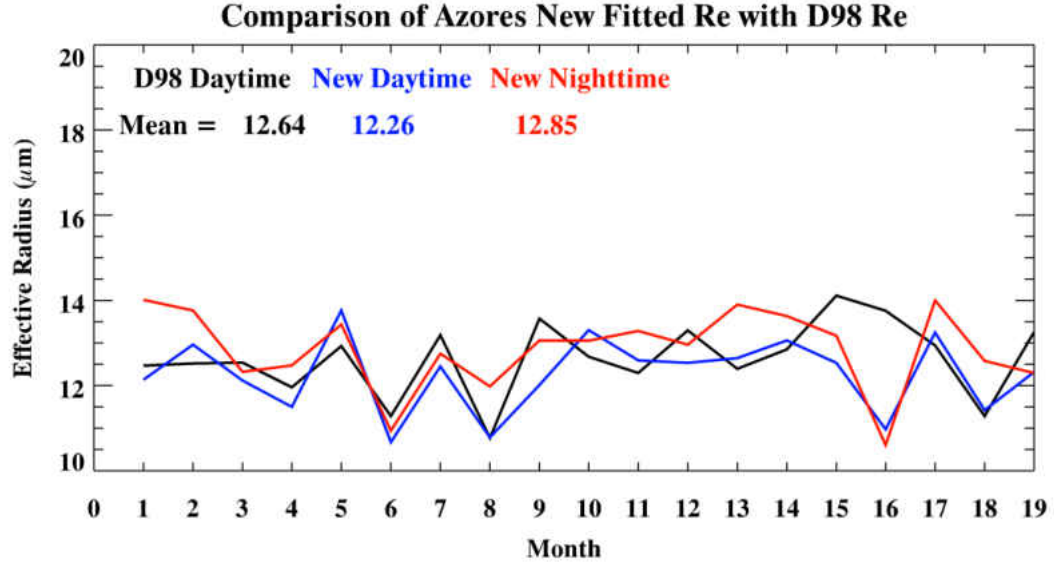
Figure 6.   Comparison of layer mean cloud-droplet effective radius calculated from D98 and Eq. (6) for the 19-month observations. Black line is daytime results from D98, blue line is daytime results from Eq. (6) and red line is nighttime results calculated from Eq. (6).

Stratocumulus Clouds under Coupled/Decoupled Boundary Layers

Six coupled, decoupled and mixed cases were selected in D15 from the 19-month AMF datasets, with each case last ~2 days long. The methods used in each case selection in D15 were from Jones et al. (2011): potential temperature profiles and Lifting Condensation Level (LCL). For the six selected cases, both methods agree reasonably well, with the potential temperature method classifying 35.5% of the samples as coupled to the surface, while the LCL method classified 36% as coupled. In this study, we extend the study of D15 to a 19-month period and use the potential temperature method only to classify coupled or decoupled samples.

The potential temperature method has been widely used to differentiate between coupled and decoupled MBL stratocumuli. For a cloud layer to be coupled with the surface, the boundary layer below the cloud layer must be well mixed. This means that turbulence is strong enough to mix the boundary layer so that properties such as mixing

22

ratio are uniform vertically. The two variables used in the potential temperature method are liquid potential temperature (θ_l) and total water content (q_t), which can be calculated using $\theta_l \approx \theta - \frac{L}{c_p} q_l$ and $q_t = q_l + q_v$, where θ is the potential temperature, L is the latent heat of vaporization for water, c_p is the specific heat of dry air at constant pressure, q_l is the liquid water mixing ratio and q_v is the water vapor mixing ratio.

As demonstrated in Fig. 7a and 7b, θ_l is nearly constant from the surface to the stratocumulus cloud base for a well-mixed boundary layer, while for the decoupled case, θ_l is not constant with height (Fig 7c).
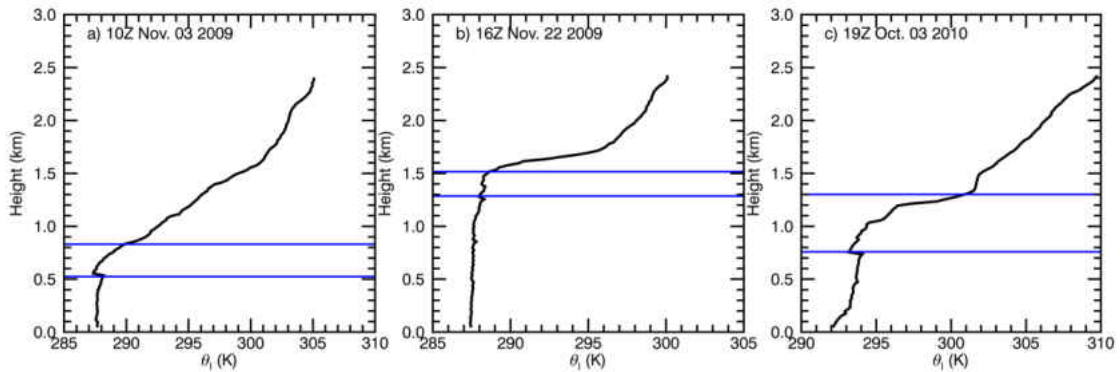
Figure 7. Liquid potential temperature (θ_l) profiles for well mixed boundary layer (a and b) and a decoupled boundary layer (c). Blue lines indicate cloud boundaries (cloud top and cloud base)

Before the potential method can be used, the sub-cloud layer must be defined. The cloud base height is used to define the top of the sub-cloud layer, which is derived from CEIL. The bottom of the sub-cloud layer is defined as the top of the surface layer, which is approximately 300 meters above ground level (AGL). The surface layer is not included in the sub-cloud layer in this study, because it is heavily influenced by surface heating/cooling fluxes. The sounding data used in this study were taken over the island, which cannot be used to represent the actual surface heating/cooling fluxes over the

ocean. Over land, the surface warms/cools more quickly than the ocean, which can lead to false signals in the vertical potential temperature profile relative to conditions over water, such as inversion layers at night. Once the sub-cloud layer is defined, the θ_l profile of this layer can be defined as either well mixed or decoupled using the threshold $\Delta\,\theta_l <$ 0.5 K as suggested in Jones et al. (2011) and used in D15. An additional criterion, the difference of q_t between the bottom 25% and top 25% of the boundary layer below the inversion was also used in Jones et al. (2011) and D15 for selecting coupled cases (also see Fig. 8 for q_t profiles in coupled and decoupled cases). As such, if the averaged θ_l and q_t differences between the bottom and top of the sub-cloud layer are less than 0.5 K and 0.5 g/kg, respectively, then the sub-cloud layer is considered to be well-mixed and identified as coupled cases. Otherwise they are identified as decoupled cases.
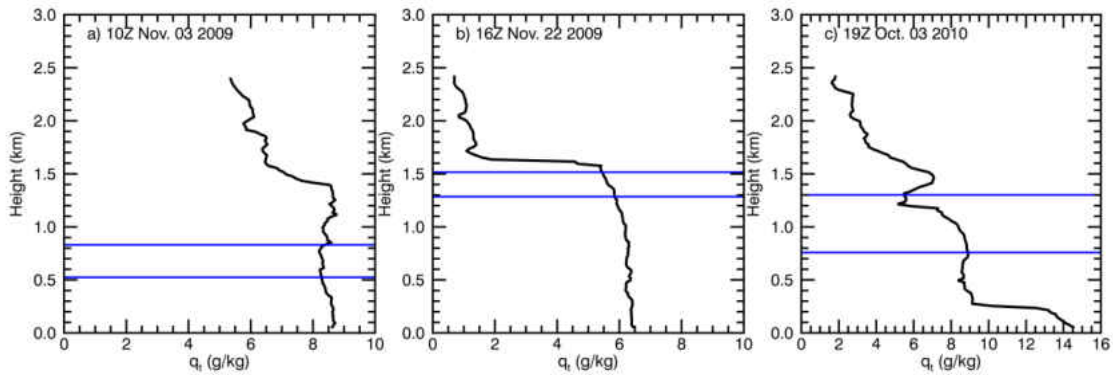
Figure 8. Total water content (q_t) profiles for well mixed boundary layer (a and b) and a decoupled boundary layer (c). Blue lines indicate cloud boundaries (cloud top and cloud base).

The criteria described above are used to identify coupled and decoupled samples during the 19-month observations. The characteristics of coupled and decoupled MBL cloud properties as well as the statistical results will be investigated (Section 3).

Drizzle Property Retrieval Algorithm

The method presented by O'Connor et al. (2005) is used to retrieve drizzle particle

effective radius, number concentration, and liquid water content. The ratio of radar

reflectivity to lidar backscatter is proportional to the fourth power of drop size, so an

accurate estimate of drizzle particle size can be provided from the ratio. Follow

O'Connor et al. (2005) and Fielding et al. (2015), we assume drizzle particle size

distribution can be represented as normalized gamma distribution of the form:

$$n(D) = N_W f(\mu) \left(\frac{D}{D_0}\right)^{\mu} \exp\left[\frac{-(3.67+\mu)D}{D_0}\right]. \tag{9}$$

where N_W is the concentration normalized, D_0 is the median diameter, μ is the shape

parameter and $f(\mu) = \frac{6}{3.67^4} \frac{(3.67+\mu)^4}{\Gamma(\mu+4)}$.

The intrinsic Doppler spectral width (σ_d) will be calculated from the drizzle size

distribution to compare with σ_d calculated from the WACR observed Doppler spectral

width (σ_v). The mean Doppler velocity ($\bar{v}$), measured by WACR, is the sum of the

vertical air motion (w) and the mean Z-weighted droplet terminal fall velocity ($\overline{v_d}$):

$$\bar{v} = w + \overline{v_d}, \tag{10}$$

$$\overline{v_d} = -\frac{\int_0^\infty n(D)D^6 v(D)dD}{\int_0^\infty n(D)D^6 dD}. \tag{11}$$

where $v(D)$ is the terminal velocity of the individual water droplets and were given by

Rogers and Yau (1989) as follows:

$$v(D) = \begin{cases} (\frac{D}{2})^2 \cdot 1.19 \times 10^6 cm^{-1} s^{-1}, & 0 < D \leq 80 \, \mu m \\ \frac{D}{2} \cdot 8 \times 10^3 s^{-1}, & 80 \, \mu m < D < 1.2 \, mm \end{cases} \tag{12}$$

σ_d can be calculated from (11) and (12):

$$\sigma_d^2 = \frac{\int_0^\infty (v(D) - \overline{v_d})^2 n(D) D^6 dD}{\int_0^\infty n(D) D^6 dD},\tag{13}$$

σ_d can also be calculated from σ_v, which is given by:

$$\sigma_d^2 = \sigma_v^2 - \sigma_b^2 - \sigma_t^2,\tag{14}$$

where σ_b^2 is the contribution due to finite beamwidth and σ_t^2 is the contribution from air turbulence. According to O'Connor et al. (2005), we use $\sigma_b = 0.032$ and $\sigma_t^2 = 0.14\sigma_v^2$ in this study.

The lidar extinction coefficient (α) is defined as $\alpha = \frac{\pi}{2}\int_0^\infty n(D) D^2 dD$. The lidar backscatter coefficient (β) is given by $\alpha = S\beta$, where S is the lidar ratio which can be estimated using Mie theory.

The ratio of radar reflectivity to lidar backscatter can be derived as:

$$\frac{Z}{\beta} = \frac{2}{\pi}\frac{\Gamma(7+\mu)}{\Gamma(3+\mu)}\frac{S}{(3.67+\mu)^4}D_0^4.\tag{15}$$

The retrieval scheme is based on an iterative approach using the radar measured spectral width as a constraint. At first, the initial D_0 can be estimated assuming $\mu=0$, and then vary D_0 by adjusting μ to calculate the radar spectral width. The final D_0 and μ values can be retrieved until the calculated radar spectral width converges to within 10% of measured radar spectral width. Once D_0 and μ values are determined, N_W can be calculated from radar reflectivity, thus, the three parameters of drop size distribution are established. Now we can calculate the drizzle LWC (LWC_d), number concentration (N_d) and effective radius (r_d) as follows:

$$\mathrm{LWC_d} = \rho_l\frac{\pi}{6}\int_0^\infty n(D) D^3 dD,\tag{16a}$$

$$N_d = \int_0^\infty n(D)\, dD,\tag{16b}$$

26

$$r_d = \frac{\int_0^\infty r^3 n(r) \, dr}{\int_0^\infty r^2 n(r) \, dr} \ .$$
(16c)

Using the error analysis method in O'Connor et al. (2005), the uncertainties of retrieved LWC_d, N_d and r_d are 10%, 13%, and 14%, respectively, in this study.

LWP_d can be calculated by integrating LWC_d through the drizzle column below cloud base. Once LWP_d is calculated, the cloud LWP (LWP_c) can be calculated by subtracting LWP_d from LWP retrieved from MWR. LWP_c is then used as input in (1) and re-run the algorithm to get the cloud properties without the impact of drizzle below cloud base. Since drizzle has little effect on solar transmission (D98), the daytime layer mean cloud particle size retrieved from (1) highly depends on LWP, which should be LWP_c rather than total LWP of the atmospheric column. So subtracting LWP_d from LWP can remain LWP_c only in the calculation, and we can get more accurate cloud microphysical properties. Note that drizzle within the cloud is out of the scope of this study and will be part of our future work.

CHAPTER III

RESULTS

Cloud Property Retrievals

The cloud microphysical properties were retrieved by the newly developed algorithm (Eq. 6) and shown in Section 2. To directly compare the daytime and nighttime MBL cloud microphysical properties, we include the daytime results from D14a. Monthly means of both the daytime and nighttime *LWP, LWC*, r_e, N_t and τ, as well as surface measured N_{CCN}, are shown in Fig. 9. Their corresponding Probability Distribution Functions (PDFs) and Cumulative Distribution Functions (CDFs) are shown in Fig. 10 and their seasonal and yearly mean, standard deviation, median, and mode values are listed in Table 2. Since daytime results calculated using D98 have been presented and discussed in great detail in D14a, we will not discuss these results in this study. Rather, we will compare the nighttime results with their daytime counterparts, and point out their similarities and differences. In Fig 9 and 10, as well as Fig. 11 discussed below, daytime microphysical properties from both D98 and Eq. (6) were included, results from Eq. (6), in general, agree well with those from D98 except for N_t. The N_t velues calculated from Eq. (6) are lower than those from D98, but the trend are the same. So the microphysical properties calculated from Eq. (6) can represent both daytime and nighttime cloud properties well. We will not compare the daytime results from two methods in the thesis,

28

in the following analysis and discussions, only the daytime microphysical properties from D98 were used.

As demonstrated in Fig. 9a (Fig. 9b), all nighttime monthly means of *LWP* exceed their daytime counterparts with an annual mean of 139.6 g m^{-2}, which is ~30.9 g m^{-2} (28.2%) larger than the daytime mean (Table 2). Because the MBL clouds are primarily driven by convective instabilities caused by cloud-top LW radiative cooling, more MBL clouds are well mixed and coupled with the surface during the night (Caldwell et al. 2005; Wood 2005a, 2005b and 2012; Schwantes, 2014; D15), thus its cloud layer is deeper and its *LWP* is higher. During the day, the cloud layer is heated by the absorption of solar radiation and partially offsets the cloud-top LW cooling, which makes MBL cloud layer thinner with less *LWP*. The seasonal variations of cloud *LWC* and optical depth basically follow the variation of *LWP*.
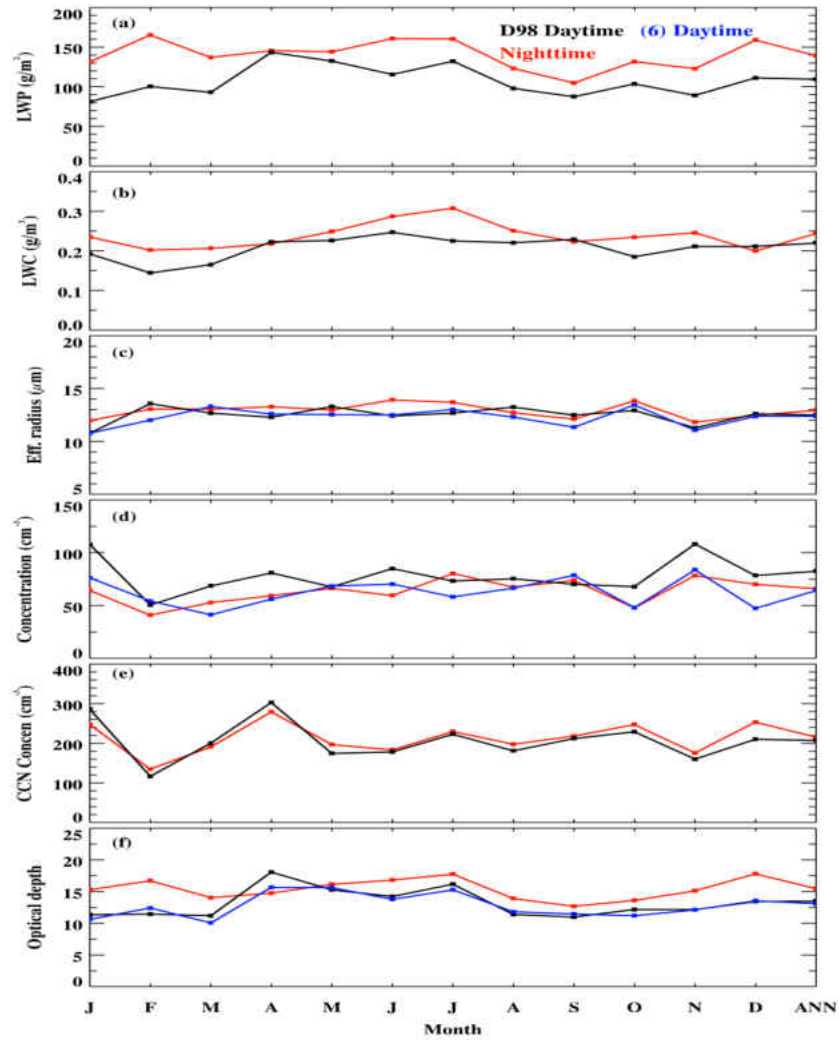
Figure 9. Monthly mean daytime (1090 hours, black line for D98 and blue line for Eq. (6)) and nighttime (1445 hours, red line) single-layered MBL cloud microphysical properties derived from 19 months of ARM Azores observations. (a) *LWP*, (b) *LWC*, (c) cloud-droplet effective radius r_e and (d) number concentration N_t, and (f) optical depth, as well as (e) surface measured CCN.
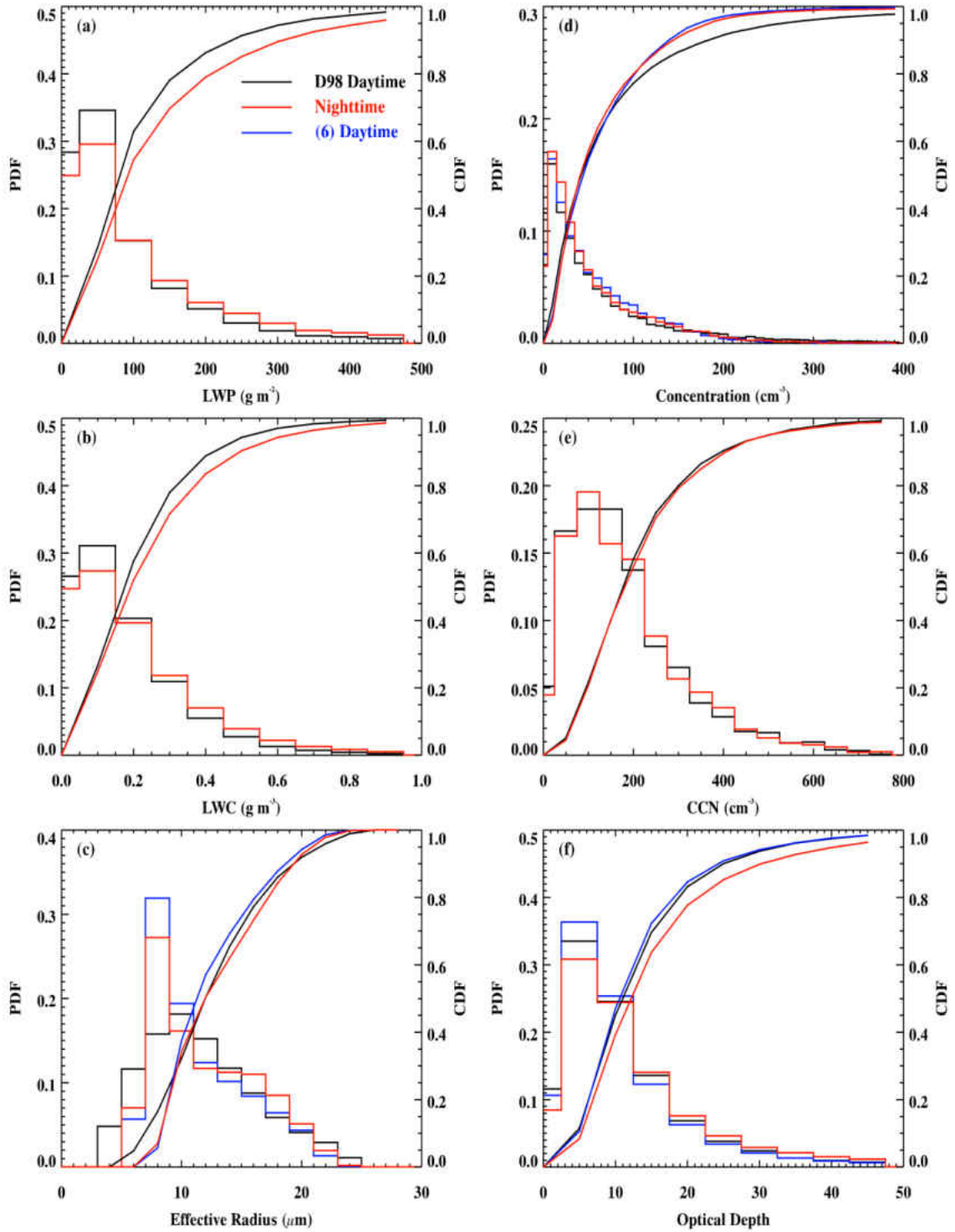
Figure 10. Probability Distribution Functions (PDF) and Cumulative Distribution Functions (CDF) of single-layered MBL cloud microphysical properties and surface CCN for both daytime (black for D98 and blue for Eq. (6)) and nighttime (red) from all 5-min samples at the ARM Azores site during the 19-month period.

31

Table 2. Seasonal and yearly averages, standard deviations, medians, and modes of various cloud parameters derived from the 19-month ARM Azores dataset (all daytime results were calculated using D98).

Winter		Spring		Summer		Autumn		Year	
Day	Night	Day	Night	Day	Night	Day	Night	Day	Night
LWP (g m^{-2})									
99.0	147.4	121.8	138.4	114.4	148.8	93.3	124.6	108.7	139.6
92.0	144.9	119.9	133.4	96.3	129.6	76.9	115.4	96.0	129.1
65.7	90.6	75.2	87.5	81.4	100.9	68.7	84.5	75.4	91.6
25	25	25	75	75	75	75	75	75	75
r_e (µm)									
12.4	12.9	12.6	13.1	12.7	13.4	13.6	12.6	12.5	12.9
5.1	3.9	4.6	4.7	4.2	4.3	4.4	4.1	4.6	4.2
11.5	12.5	12.0	11.4	11.2	12.4	12.7	11.8	11.9	11.9
9	9	11	9	11	9	11	9	11	9
N_t (cm^{-3})									
75.4	63.4	76.8	64.9	82.5	65.9	89.1	68.1	82.6	66.0
117.7	125.0	113.4	68.7	137.9	65.9	110.8	103.2	126.2	96.0
36.3	37.5	40.3	44.8	43.5	44.2	52.4	39.7	44.1	41.0
5	15	15	15	15	15	15	15	15	15
N_{CCN} (cm^{-3})									
265.6	236.9	235.3	231.8	192.5	206.7	196.1	206.6	207.3	215.9
222.7	198.8	195.9	212.8	109.8	113.6	114.8	125.1	143.8	153.8
173.9	173.7	162.7	160.8	173.8	193.1	180.4	181.3	175.0	181.3
125	125	75	75	125	125	175	125	125	125
τ									
12.1	16.5	14.9	15.2	14.0	15.0	12.1	16.3	13.5	15.5
8.4	12.6	12.7	9.3	9.7	12.1	7.3	12.5	9.6	12.1
10.0	13.1	10.9	9.8	11.4	11.1	10.5	12.7	11.0	11.9
7.5	7.5	7.5	7.5	7.5	7.5	7.5	7.5	7.5	7.5

The nighttime monthly means of r_e are nearly the same as their daytime counterparts, and both daytime and nighttime r_e values are nearly constant throughout the year. As listed in Table 2, the nighttime annual mean of r_e is 12.9 µm (roughly 0.4 µm larger than its daytime mean) and the nighttime average, standard deviation, median, and mode values are nearly the same as the daytime counterparts with the differences less than 2 µm. The nighttime PDF and CDF r_e values are similar to the daytime PDF and CDF trends (Fig. 10c) except for a peak at 8-10 µm. This is consistent with the mode value of

9 μm in Table 2, while the daytime mode value is 11 μm. Because τ was calculated from (8) (i.e., the ratio of LWP to r_e), the monthly means basically follow the LWP variation since r_e is nearly constant throughout the year. Table 2 shows that the day-night differences in τ are more than 4 during the winter and autumn months while the annual mean difference is 2.

The nighttime monthly means of N_t fluctuate around an annual mean of 65.9 cm^{-3} with a minimum of 41 cm^{-3} in February and a maximum of 80.3 cm^{-3} in July. Although the nighttime PDF and CDF look like almost identical to the daytime counterparts, nighttime has more low values as shown in Fig. 9 and listed in Table 2. Both the nighttime and daytime monthly means of surface N_{CCN} and the corresponding PDFs and CDFs are nearly identical as well.

Figure 11 shows the hourly means of LWP, LWC, r_e, N_t, N_{CCN}, and τ for the 19-month period. As discussed above and in D14a, there are larger nighttime LWP values (140 gm^{-2}) than daytime (109 gm^{-2}) suggesting a semi-diurnal cycle with maxima occurring at 0500 LT and 2100 LT, respectively. Because diurnal variations in cloud thickness (D14a) and r_e are small, hourly means of LWC and τ are primarily determined by LWP (Figs. 11b and 11f).
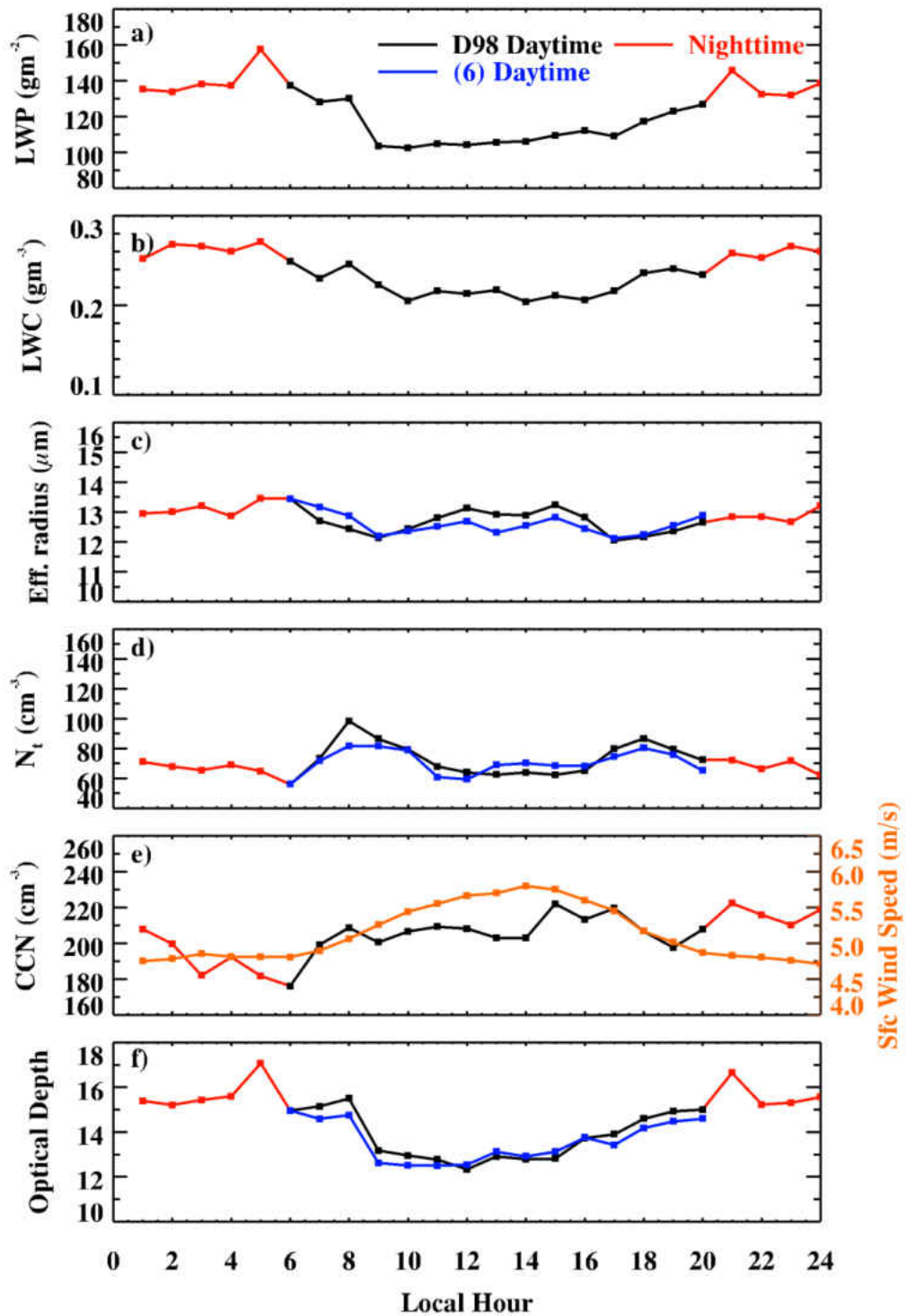
Figure 11. Hourly means of single-layered MBL cloud microphysical properties from both daytime and nighttime datasets. The daytime and nighttime are shown in each panel with black (D98), blue (Eq. (6)) and red lines, respectively. The orange line in e) is surface wind speed (10 m).

Figure 11e illustrates that the hourly means of N_{CCN} dramatically decrease from midnight (~ 210 cm^{-3}) to sunrise (176 cm^{-3}) at 0600 LT, immediately increase to 200-210 cm^{-3} during the 0700-1400 LT period, and then jump to ~220 cm^{-3} during late afternoon and night. Therefore, we can conclude that there is an increase in surface CCN from around sunrise (0300-0600 LT) to late afternoon and night at the Azores. By analyzing the hourly means of surface wind speed (10 m, Fig. 11e), the wind speed increases from 4.8 m s^{-1} around sunrise to 5.8 ms^{-1} at 1400 LT, suggesting a moderate correlation (r=0.76) between surface N_{CCN} and wind speed. As discussed in Logan et al. (2014), the surface aerosol properties at the Azores are well correlated surface wind speed with the greatest contribution from sea salt, but with periodic contribution from continental aerosol sources.

Although surface CCN measurements are primarily influenced by surface wind speed, precipitation may also be a factor. Hourly means of N_t follow N_{CCN} variations from midnight to 0900 LT, but not for afternoon and evening. The averaged ratio of N_t to N_{CCN} is 0.35 with higher ratios of 0.45 and 0.41 at 0800-0900 and 1800-1900 LT, respectively, and lower ratio of 0.31 at local noon. This is likely due to a higher frequency of well-mixed MBLs during the early morning and late afternoon while more decoupled MBLs typically occur near local noon. Thus, further study is necessary.

Cloud Properties under Coupled/Decoupled Boundary Layers

Using the methodologies described in the previous section, a total of 824 hours (183 and 641 hours for coupled and decoupled samples, respectively) were chosen. In this section, we will show three individual cases in detail (Figs. 12-14).
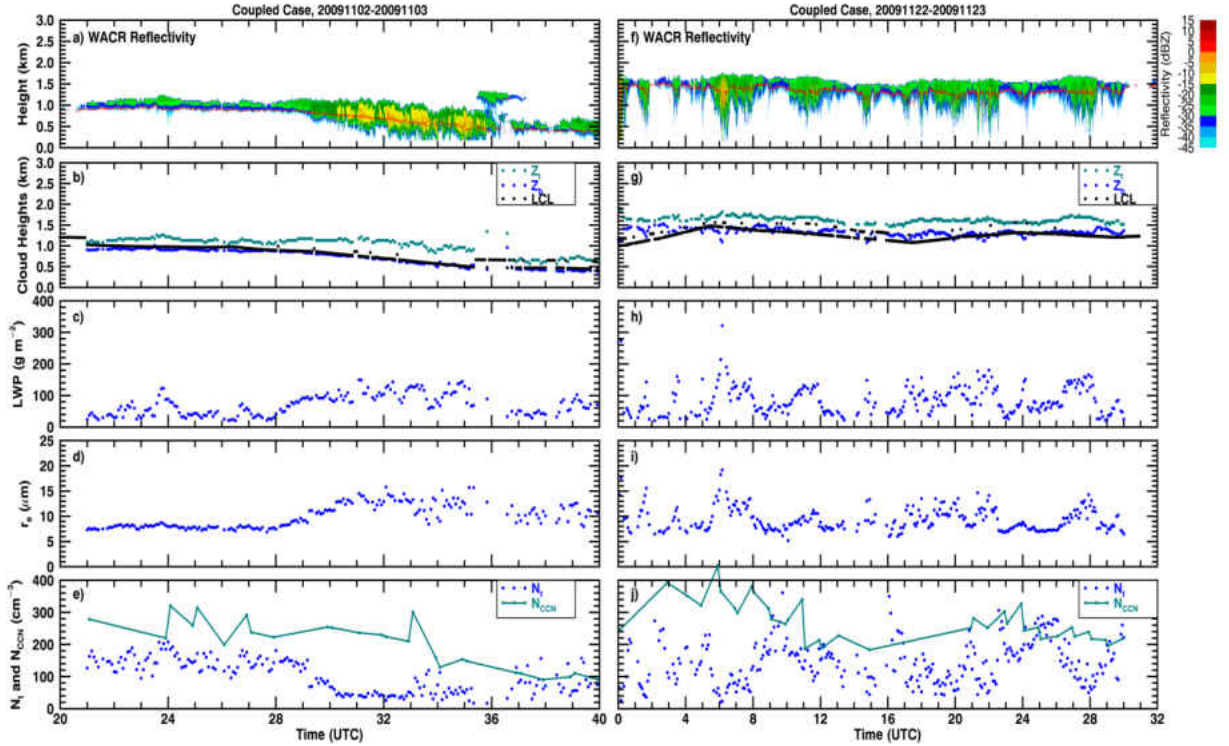
Figure 12. Time series of (Case I, a) ARM 95 GHz cloud radar reflectivity, the red line is the cloud-base height derived from ARM laser ceilometer, (b) cloud-base (Z_b) –top (Z_t) heights derived from ARM radar-lidar measurements and lift condensation level (LCL) height, (c) cloud liquid water path (*LWP*) retrieved from microwave radiometer, (d) layer mean cloud-droplet effective radius (r_e) and (e) number concentration (N_t) and corresponding surface measured cloud condensation nuclei (CCN) concentration (N_{CCN}) under the coupled condition from 2000Z 02 November 2009 to 1600Z 03 November 2009 and (Case II, f-j) from 0000Z 22 November to 0800Z 23 November 2009 at the ARM Azores site.

Figure 12 shows the MBL cloud boundaries and properties for two coupled cases, named as Cases I and II. Although we do not compare the methods of potential temperature and LCL, we included LCL height in Fig. 12 and 13 for reference. The identifications using these two methods agree very well in the coupled cases (Fig. 12) and for most time periods in the decoupled case (Fig. 13). As shown in Fig. 12a and 12b, the radar reflectivity and MBL cloud boundaries of Case I have demonstrated that the cloud layer was uniform with a depth of ~300 m (Z_b ~ 0.9 km, Z_t ~ 1.2 km) from 2000Z 02 November 2009 to 0500Z 03 November 2009. After that, the cloud layer became deeper

and cloud-base height Z_b became lower with virga occurring until 1200Z 03 November, and finally thinned out. For Case II, the radar reflectivity (Fig. 12f) clearly showed the mesoscale cellular convection (MCC) structure of the stratocumulus layer oscillating between low radar reflectivity (non-drizzle) and high radar reflectivity (drizzle) every ~2-4 hours, which is consistent with the findings of Miller et al. (1995). Virga was present for most of the time, and may be a dominant factor for maintaining MBL stratocumuli by providing a moisture source. The cloud-top Z_t and -base Z_b heights were relatively constant (~1.6 km and ~1.3 km), resulting in a nearly constant cloud thickness (~300 m) throughout the entire period (Fig. 12g).

High (low) LWPs coincided with high (low) radar reflectivity measurements and thick (thin) cloud thicknesses (Figs. 12c and 12h). For these two coupled cases, no heavy precipitation occurred because most LWP values remained below 150 g m^{-2}. The layer-mean r_e values followed the variation of LWP, with small values coinciding with low reflectivity and large values coinciding with high reflectivity (Figs. 12d and 12i). The layer mean N_t values, however, showed a negative correlation with LWP and r_e values, indicating that lower (higher) N_t values corresponded to higher (lower) LWP and r_e values. Most N_t values were below 300 cm^{-3} (Figs. 12e and 12j), and dropped below 100 cm^{-3} for drizzle events due to the collision and coalescence of cloud droplets by drizzle within the cloud layer. Most surface-measured N_{CCN} values remained relatively constant around 300 cm^{-3} except for the last 6 hours for Case I (Fig. 12e) and varied from 200 to 400 cm^{-3} for Case II (Fig. 12j).
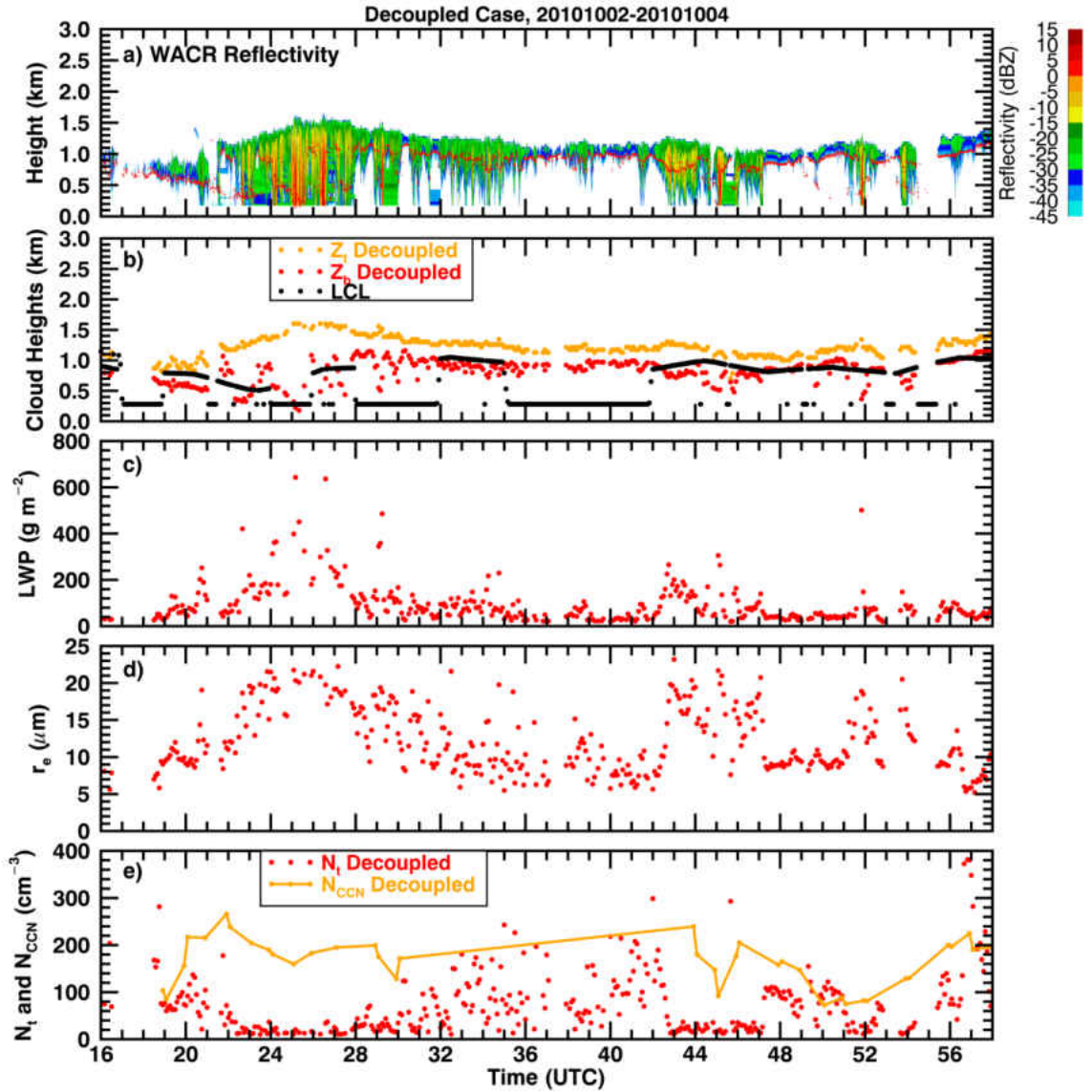
Figure 13. Same as Figure 12 except for the decoupled case (Case III), which occurred from 16Z 02 October to 10Z 04 October 2010 at the ARM Azores site.

The third case (Case III), which occurred on 02-04 October 2010, was decoupled for the entire period (Fig. 13). The radar reflectivity also showed a MCC structure that has similar characteristics to Case II, but has significant differences, such as several periods with rain reaching the surface and thickened cloud layer. This is in contrast with Case I and Case II where the cloud layer was solid and uniform with virga falling out Z_b. Z_t, and Z_b fluctuated frequently with deep cloud layers during heavy drizzle periods and shallow

cloud layers during non-drizzle periods (Fig. 13b). Note in this panel that some periods of the LCL heights in this case were almost constant and stay around 300m. We found from the merged sounding data that there was always a stable layer at around 300m, and even though we used temperature and dew point temperature 300m AGL, the calculated LCL height still exhibit relatively constant periodically. Further study is needed to find out reasonable explanations about the stable layer in merged sounding data. The averages of Z_t and Z_b were 1.22 km and 0.81 km, respectively, and the maximum Z_t reached 1.7 km and the minimum Z_b was 0.3 km, resulting in a large fluctuation of cloud layer depth. This is in contrast to Case I and Case II where Z_t and Z_b values were kept nearly constant due to lack of heavy drizzle events. LWP values also had large fluctuations with values greater than 200 g m^{-2} when heavy drizzles and deep cloud layers occurred (Fig. 13c). The r_e values followed the variation of LWPs, with larger r_e values during the precipitation periods than those during non-drizzle periods. It is evident that both LWP and r_e values in this case are larger than those in Cases I and II (Fig. 12). Their corresponding N_t and N_{CCN} values, however, are much lower than those in Cases I and II, especially during the heavy drizzle periods. N_{CCN} values were also significantly low for this case, with most of N_{CCN} values being below 200 cm^{-3} (Fig. 13e) while they were more than 200 cm^{-3} for Case I and Case II (Figs. 12e and 12j).

The PDFs and CDFs of coupled and decoupled MBL cloud macro- and micro-physical properties from the selected samples are shown in Fig. 14. Furthermore, we compare these coupled and decoupled cloud properties under non-drizzle and drizzle (virga and rain) conditions, and during daytime and nighttime periods. Their corresponding means are listed in Table 3. Out of a total of 9888 5-min samples, 22.2%

were classified as coupled and 77.8% as decoupled; 32.7% as non-drizzle and 67.3% as drizzle (48.7% as virga, 18.6% as rain); 40.6% as daytime and 59.4% as nighttime. The decoupled samples have a higher frequency (68%) of drizzling events compared to the coupled samples (58%). Drizzling events are dominant for both daytime (59%) and nighttime (67%) samples in this study.

Table 3. Means of all coupled and decoupled samples

	Z_b (km)	Z_t (km)	ΔZ (km)	T_{cldy} (K)	LWP (g m^{-2})	r_e (µm)	N_t (cm^{-3})	N_{CCN} (cm^{-3})
Coupled	0.77	1.1	0.33	286.6	116.4	11.9	102.2	210.8
Decoupled	1.1	1.5	0.4	285.2	135.1	12.7	80.6	180.9

Figure 14 shows the PDFs and CDFs of the MBL stratocumulus cloud macrophysical and microphysical properties for both coupled (blue) and decoupled (red) samples. The PDF distributions of coupled and decoupled Z_b are different. The mode value occurs around 0.8-1.4 km for decoupled samples, whereas a bimodal distribution is found for coupled samples with mode values of 0.6-0.8 km and 1.2-1.4 km. Listed in Table 3, the averaged Z_b for coupled samples is 0.77 km, which is about 0.4 km lower than the mean value of decoupled samples. The coupled and decoupled PDF distributions of Z_t are similar to their Z_b counterparts with a range of 0.4 km higher, in addition to modal values of 1.2-2 km for decoupled samples, and 1.0-1.2 km for coupled samples. The averaged Z_t for coupled samples is 1.081 m, which is about 0.462 km lower than the mean value of decoupled samples. As a result, the averaged cloud layer depth ΔZ for coupled samples is only 0.33 km, which is about 0.07 km thinner than the mean value of

decoupled samples. The decoupled cloud layer depth distribution is slightly more skewed towards higher values (35% for $\Delta Z > 0.5$ km) compared to the coupled distribution (only 16% for $\Delta Z > 0.5$ km). The mean cloud temperatures have a broad distribution from 0 $^{\mathrm{o}}$C to 20 $^{\mathrm{o}}$C.
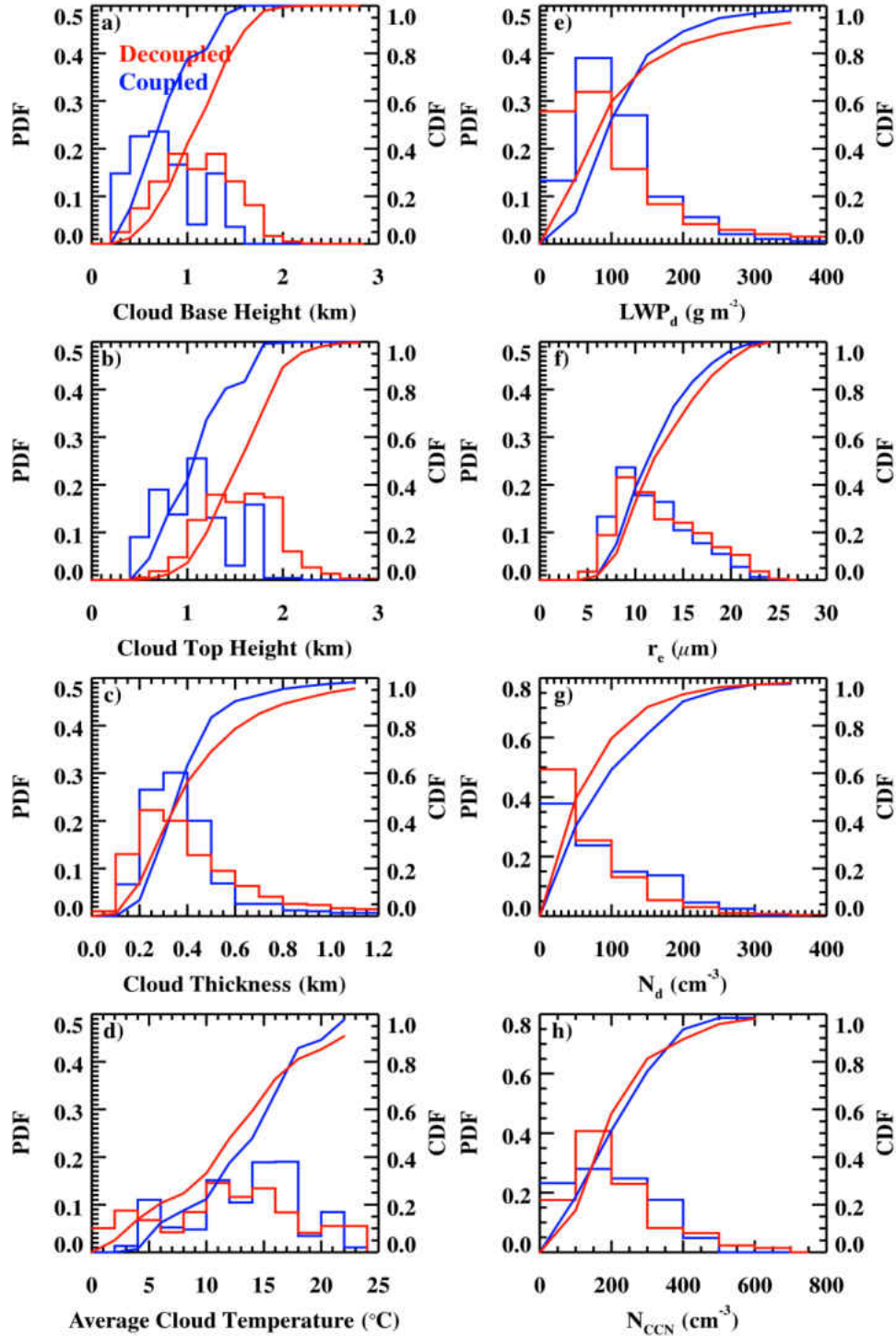
Figure 14. Probability distribution functions (PDF) and cumulative distribution functions (CDF) of (a) cloud-base height (Z_b), (b) cloud–top height (Z_t), (c) cloud thickness, (d) averaged cloud temperature, (e) LWP, (f) r_e, (g) N_t, and (h) N_{CCN} from coupled (blue) and decoupled samples (red) from 19-month samples.

Figures 14e-h show the PDFs and CDFs of the MBL cloud microphysical properties, such as LWP, r_e, N_t and the corresponding surface-measured N_{CCN}. The LWP and r_e distributions for decoupled samples are skewed to higher values compared to those from coupled samples. The decoupled LWP distribution has 21% of its values greater than 150 g m^{-2} while the coupled LWP distribution has 19% of its values above 150 g m^{-2}. Coupled and decoupled r_e values have similar distributions with decoupled r_e skew slightly towards higher values. For both conditions, the mode values are 8-10 μm. On average, the decoupled stratocumuli have higher LWP and r_e values (135.1 g m^{-2} and 12.7 μm) compared to the coupled stratocumuli (116.4 g m^{-2} and 11.9 μm) because more drizzle events occur when the cloud layer is decoupled. In contrast to their LWP and r_e distributions, the decoupled distributions of N_t and N_{CCN} are skewed to lower values compared to their coupled distributions. About 70% of the decoupled N_t values are lower than 100 cm^{-3}, while only 57% of values are in this range for the coupled N_t values below 100 cm^{-3} due to the following two reasons. The first reason is that decoupled stratocumuli do not have N_{CCN} coming from the surface, which does not allow more cloud droplets to form. The second reason might be that drizzle occurrences are higher for decoupled periods (68%) than for coupled periods (58%), though fewer cloud drops might also be the reason of more drizzle. Drizzle is formed through the collision and coalescence of cloud droplets, suggesting that the number of cloud droplets is greatly reduced when drizzle is present within a cloud layer.

The statistical results of the coupled and decoupled cloud parameters under non-drizzle and drizzle (virga and rain), and during daytime and nighttime periods are listed in Table 4. The averages of coupled and decoupled Z_b under non-drizzle condition

are 0.74 km and 1.1 km, respectively, which is close to the virga averages (0.85 km and 1.2 km) but much higher than the rain averages (0.54 km and 0.84 km). The corresponding averages of coupled and decoupled Z_t are 0.94 km and 1.4 km for non-drizzle, 1.2 km and 1.6 km for virga, and 1.1 km and 1.6 km for rain. In general, the Z_t differences for non-drizzle, virga and rain are insignificant, however, the Z_b values of rain are much lower than those of non-drizzle and virga. Therefore, the cloud layer depths under non-drizzle and virga are close to each other, but more than 200 m shallower than those of rain.

Table 4. Means of coupled and decoupled samples under non-drizzle and drizzle (virga and rain) conditions

		Z_b (km)	Z_t (km)	ΔZ (km)	T_{cldy} (K)	LWP (g m^{-2})	r_e (μm)	N_t (cm^{-3})	N_{CCN} (cm^{-3})
Non-Drizzling	Coupled	0.74	0.94	0.2	288.2	77.1	10.0	123.3	239.1
	Decoupled	1.1	1.4	0.3	287.6	96.3	11.2	111.9	204.5
Drizzling — Virga	Coupled	0.85	1.2	0.35	284.2	98.3	11.9	90.6	216.0
	Decoupled	1.2	1.6	0.4	283.4	118.5	12.8	78.1	205.9
Drizzling — Rain	Coupled	0.54	1.1	0.56	287.0	206.3	15.1	44.0	90.7
	Decoupled	0.84	1.6	0.76	283.5	329.4	18.0	27.6	99.8

The averages of coupled and decoupled LWPs under non-drizzle condition are 77.1 gm^{-2} and 96.3 gm^{-2}, slightly less than the averages (98.3 g m^{-2} and 118.5 g m^{-2}) of virga, but significantly less than the averages (206.3 g m^{-2} and 329.4 g m^{-2}) of rain. The comparisons of coupled and decoupled r_e values for non-drizzle, virga and rain mimic the

LWP comparisons, i.e., the averages of non-drizzle and virga r_e are close to each other, but much less than those of rain. In contrast to *LWP* and r_e comparisons, the averages of coupled and decoupled N_t under non-drizzle condition are 123.3 cm^{-3} and 111.9 cm^{-3}, which is higher than the averages (90.6 cm^{-3} and 78.1 cm^{-3}) of virga, but they are approximately 3-4 times as high as the averages (40 and 27.6 cm^{-3}) of rain. Similar trends have also been observed for N_{CCN}. These results have indicated that the MBL cloud microphysical properties under non-drizzle and virga conditions are similar to each other, but significantly different to those of rain.

Table 5. Means of coupled and decoupled samples during daytime and nighttime periods

		Z_b (km)	Z_t (km)	ΔZ (km)	T_{cldy} (K)	LWP (g m^{-2})	r_e (μm)	N_t (cm^{-3})	N_{CCN} (cm^{-3})
Daytime	Coupled	0.85	1.1	0.25	289.1	102.3	11.1	96.4	196.5
	Decoupled	1.2	1.5	0.3	286.2	113.7	12.7	100.6	194.4
Nighttime	Coupled	0.84	1.2	0.36	285.1	118.0	11.4	105.5	220.0
	Decoupled	1.1	1.6	0.477	284.5	156.7	13.6	67.6	221.4

For daytime and nighttime comparisons, the averaged Z_b and Z_t differences are less than 100 m for coupled and decoupled samples (Table 5). There is no significant difference between coupled and decoupled *LWP* values (102.3 g m^{-2} vs. 113.7 g m^{-2}) during the daytime, but a large difference (118 g m^{-2} vs. 156.7 g m^{-2}) is found during the nighttime. The diurnal variation in LWP has resulted in corresponding r_e differences. For example, the coupled and decoupled r_e values are 11.1 μm and 12.7 μm during the daytime, but for the nighttime the r_e difference can be up to 4 μm (11.4 μm vs. 13.6 μm).

Corresponding to its largest r_e value, the nighttime decoupled N_d (67.6 cm^{-3}) is much less than others.

The statistical results of coupled and decoupled samples, in general, are consistent with the results in D15, except that the Z_b and Z_t values for coupled samples are lower those in D15. This is reasonable because there are more coupled samples in this study than those in D15. The statistics of microphysical properties are consistent with those in D15.
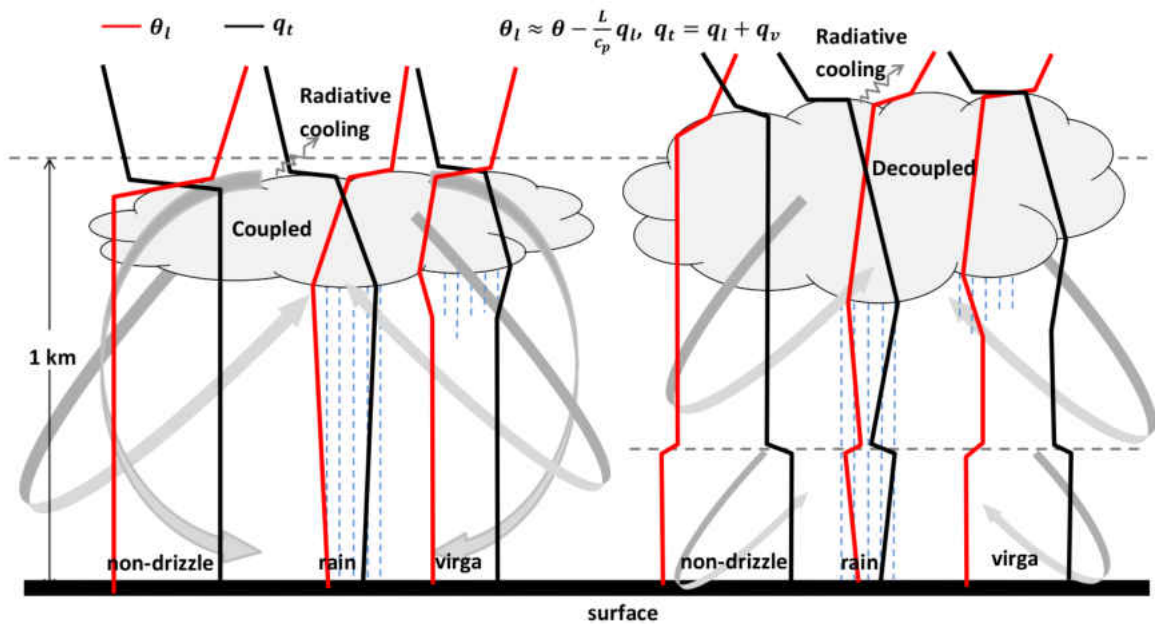
Figure 15. A schematic diagram to show the characteristics of coupled and decoupled boundary layer when the stratocumulus cloud appeared at the top of boundary layer.

To summarize our findings, we plot a schematic diagram to show the characteristics of coupled and decoupled MBL in Fig. 15. For coupled samples, the liquid water potential temperature θ_l and total water mixing ratio q_t are conserved throughout the stratocumulus topped boundary layer (STBL) when non-drizzle occurs, and both variables change sharply above Z_t due to dry air above it. With the drier air above Z_t, the decrease of q_t results in an increase of stability and decrease of q_l further,

then θ_l starts to increase sharply. When rain occurs, q_l is greater than zero below Z_b, thus θ_l decreases and q_t increases from the surface to Z_b. Within the cloud layer, q_t decreases and θ_l increases from Z_b towards Z_t due to the depletion of rains. For virga, both θ_l and q_t are conserved from the surface to the drizzle base, and q_l is greater than zero and increases from the drizzle base to Z_b, but θ_l decreases. Within the cloud layer, the situation is the same as rain. For decoupled samples, the boundary layer is deepened and separated into two layers (dashed line in Fig. 15) with its own circulation in each layer. The surface moisture cannot be transported into the upper layer where the cloud stays, q_t decreases but θ_l increases in the upper layer compared to the surface mixed layer. The profiles of θ_l and q_t in the upper layer should have similar patterns to the coupled samples but change quickly due to the deepened cloud layer and without surface moisture supply.

Drizzle Property Retrievals

Figure 16 demonstrates the virga and rain below cloud base from two selected cases along with their retrieved microphysical properties. Case I represents a typical virga case occurring on 22 November 2009, and Case II is a typical rain case that occurred from the late afternoon of 8 November to the morning of 9 November 2010. Figures 17a and 17e present the WACR reflectivity profiles and the CEIL measured cloud-base heights for Cases I and II, respectively. Both cases have significant time periods when the radar reflectivities are greater than -37 dBZ below cloud base, but this happened more frequently in Case II than in Case I. Compared Fig. 16a with Fig. 16e, the radar reflectivities are generally lower in Case I than in Case II. The retrieved r_d values (Fig.

16b) are relatively smaller in Case I than in Case II (Fig. 16f), but the N_d values are higher in Case I (Fig. 16c) than in Case II (Fig. 16g).
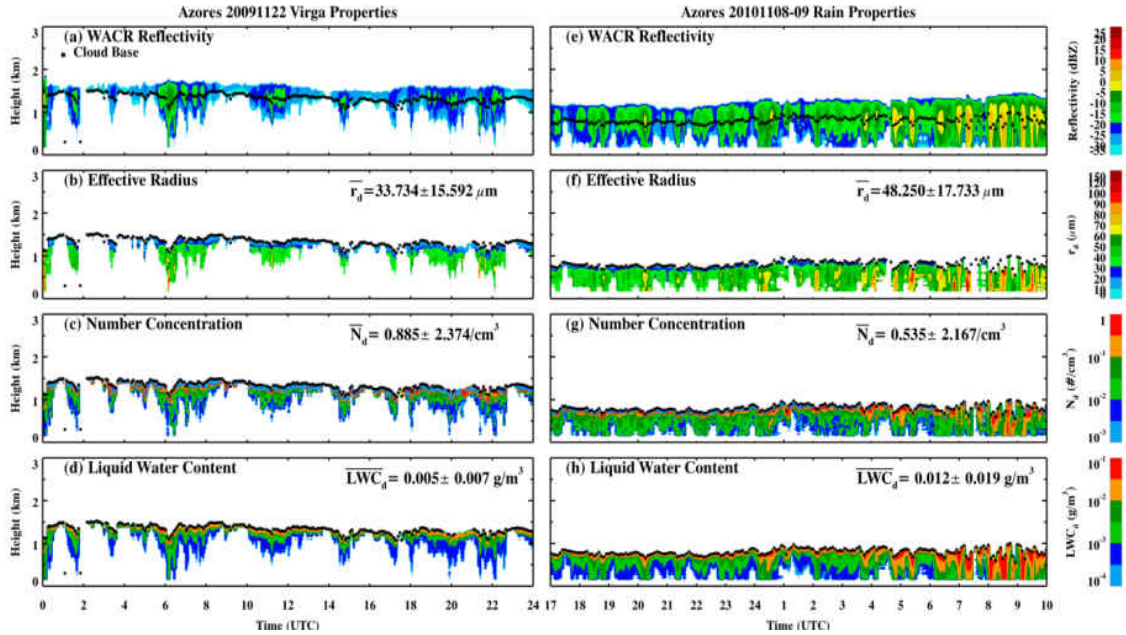
Figure 16. Drizzle properties observed by ARM radar-lidar and retrieved from this study at the ARM Azores site. Two cases have been selected: Case I (left panel, Nov. 22, 2009) is a typical virga case, and Case II (right panel, from late afternoon of November 8, 2010 to the morning of November 9, 2010) is a rain case (drizzle reaches the surface).

The mean r_d in Case I is 33.73 μm with a range of ~20-50 μm, while it is 48.25 μm for Case II, ranging from 20 to 100 μm. The larger r_d and lower N_d in Case II are anticipated because drizzle particle sizes are larger when relatively intense drizzling occurs. For example, the r_d values range from 50 to 100 μm during the period of 7-10 UTC in Case II. The mean values of r_d in both Cases are nearly 3-4 times larger than the mean values of MBL cloud-droplet effect radius r_e at the Azores (12.5-12.9 μm, D14a and D14b). However, their mean N_d values of 0.885 and 0.535 cm^{-3} are two orders of magnitude lower than the mean values of MBL cloud-droplet number concentration N_t at the Azores (66-82.6 cm^{-3}, D14a and D14b). The retrieved r_d and N_d values in both cases are also in the same magnitude as some previous studies (e.g., O'Connor et al., 2005;

Frisch et al., 1995; Wang, 2002). The drizzle LWC (LWC_d) below cloud base are about 1-2 orders of magnitude lower than the cloud LWC (LWC_c) above cloud base (shown in Table 3 of D14a), and slightly higher in Case II.

High radar reflectivity normally results from large particles because radar reflectivity is proportional to the sixth power of particle size. Figures 16b and 16c show that the r_d values below cloud base are vertically invariant, however, the N_d values decrease significantly toward to the surface, indicating that the evaporation of the drizzle particles below cloud base occurs for virga. For Case II, the r_d values increase toward the surface, but the N_d values remain either relatively constant or slightly decrease, which may be a result of the collision-coalescence process for rain. It is also notable that a narrow band appears just below the cloud base, called a "transition layer" from cloud to drizzle, which makes the r_d values smaller and the N_d values higher than those at lower levels.
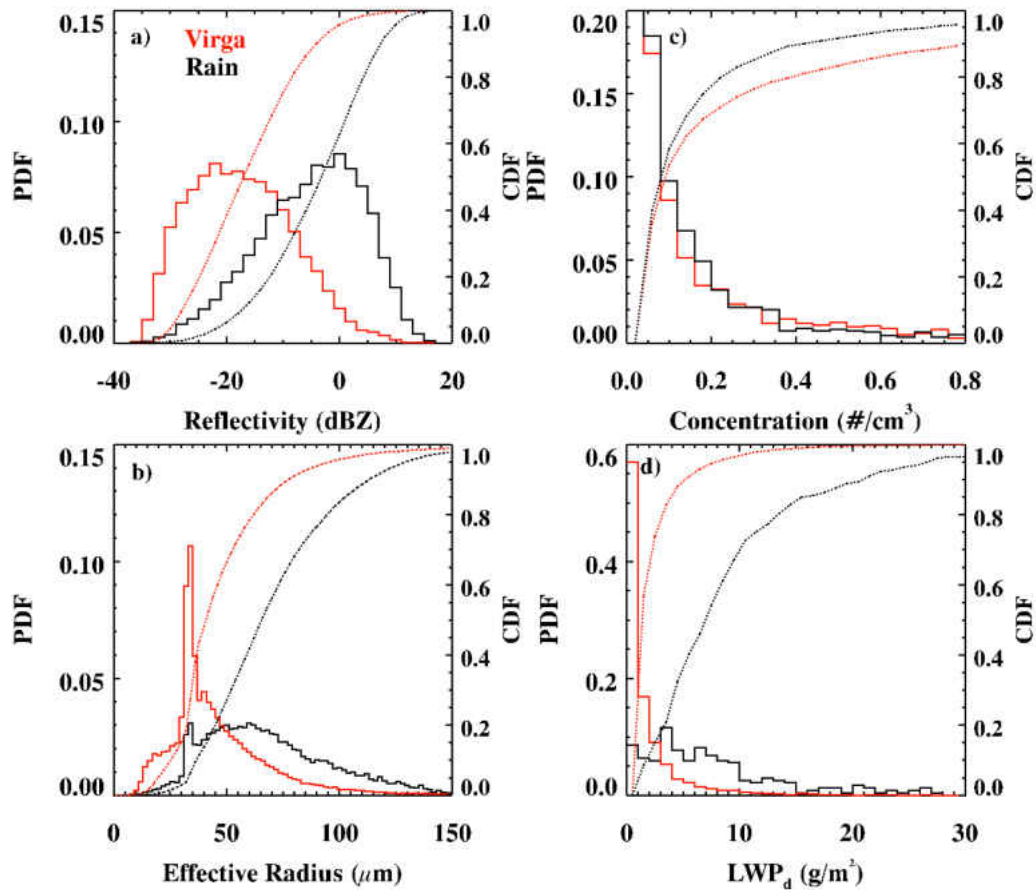
Figure 17. PDFs and CDFs of daytime drizzle properties at the Azores during the period from June 2009 to December 2010. PDFs and CDFs of (a) WACR reflectivities below cloud base for drizzle from virga and rain in this study, (b) drizzle particle effective radius r_d, and (c) number concentration N_d, and (d) liquid water path (LWP_d). The red lines and black lines represent the results from the selected virga and rain episodes, respectively.

To provide statistical results of drizzle microphysical properties and investigate to what extent drizzle impacts cloud property retrievals, we plot Figs. 17 and 18, and list their seasonal means in Table 6 and Table 7. Figure 17 shows the PDFs and CDFs of drizzle properties from a total of 353 hours of virga and 112 hours of rain samples during the 19-month period. As illustrated in Fig. 17a, the reflectivities of rain are generally higher than those of virga with the mode values of 0 dBZ and -20 dBZ, respectively. The mode value (0 dBZ) of rain is consistent with the definition of intense precipitation type

in Rémillard et al. (2012). From the CDFs of Fig. 17a, 55% of the virga and 13% of rain samples are less than -15 dBZ, and 37% of the virga and 6% of the rain samples are less than -20 dBZ. Thus, ~45% of the drizzle samples would be missed if using a threshold of -15 dBZ, and ~30% for -20 dBZ. Therefore, we conclude that a significant amount of drizzle samples would be missed if using radar reflectivity as a threshold, or a lower threshold need to be selected.

The PDFs and CDFs of drizzle particle effective radius r_d are shown in Fig. 17b. The mode value of virga samples is ~30 μm, whereas it is not so obvious for rain samples with a broad range of 30~150 μm. Nearly 66% of the virga samples are less than 50 μm and 83% of the rain samples are less than 100 μm, both with long tails towards large values. In contrast to the distributions of r_d, most of the N_d values for both virga and rain samples are located at the tail end with nearly 70-80% less than 0.2 cm^{-3} and slightly more virga samples for large values. Almost all virga LWP_d values are less than 10 g m^{-2} and ~80% less than 3 g m^{-2}, while only 18% of the rain samples are less than 3 g m^{-2}.

Impact of Drizzles on Cloud Property Retrievals

To investigate the impact of drizzle on cloud property retrievals, the cloud liquid water path (LWP_c) is calculated by subtracting LWP_d from the microwave radiometer retrieved LWP, and then used it as an input for (1) to retrieve new MBL cloud microphysical properties, $r_e{}'$, $N_t{}'$, and τ' without drizzle effect. These newly retrieved cloud properties ($r_e{}'$, $N_t{}'$, τ') are then compared with the original retrievals in D14a where the LWP was used as LWP_c in (1). Figure 18 shows the dependence of the differences between newly and originally retrieved r_e and τ on LWP_d where both Δr_e and $\Delta\tau$ linearly decrease with increased LWP_d. The slope of the linear regression line (Δr_e vs. LWP_d) for

the virga samples is 0.1 with a correlation coefficient (R^2) of 0.987 (Fig. 19a), that is, r_e

decreases 0.1 µm at an increase of 1 g m^{-3} in LWP_d. The r_e values will decrease by up to

0.3 µm with an increase of 3 g m^{-3} in LWP_d, which is within the uncertainty (~10%) of

originally retrieved r_e values in D14a. The impact of drizzle on cloud optical depth

retrieval (Fig. 18b) is similar to that of r_e with a slope of -0.02 and R^2 of 0.901. For the

rain samples, the slope is -0.07 and the correlation is 0.896. The r_e values can be reduced

2~3 µm with an increase of 40 g m^{-2} in LWP_d and relatively larger fluctuation than for the

virga samples. The impact of LWP_d on cloud optical depth retrieval is weak with a R^2 of

0.568.

A 95% confidence interval for each regression line is computed, indicating that the

true best-fit line for the samples lies within the 95% confidence interval. The two dashed

lines in Fig. 18 represent the upper and lower 95% confidence bounds for each of the

regression. The narrow intervals for Figs. 18a, 18b, and 18c suggest high reliability of the

regression, whereas for the broad interval in Fig. 18d indicates relatively large

uncertainty of the regression.

Virga Regions   **Rain Regions**

a)
$\Delta r_e = -0.1\ LWP_d - 0.002$
$R^2 = 0.987$

c)
$\Delta r_e = -0.072\ LWP_d - 0.002$
$R^2 = 0.896$

b)
$\Delta \tau = -0.02\ LWP_d - 0.002$
$R^2 = 0.901$

d)
$\Delta \tau = -0.006\ LWP_d - 0.0005$
$R^2 = 0.568$
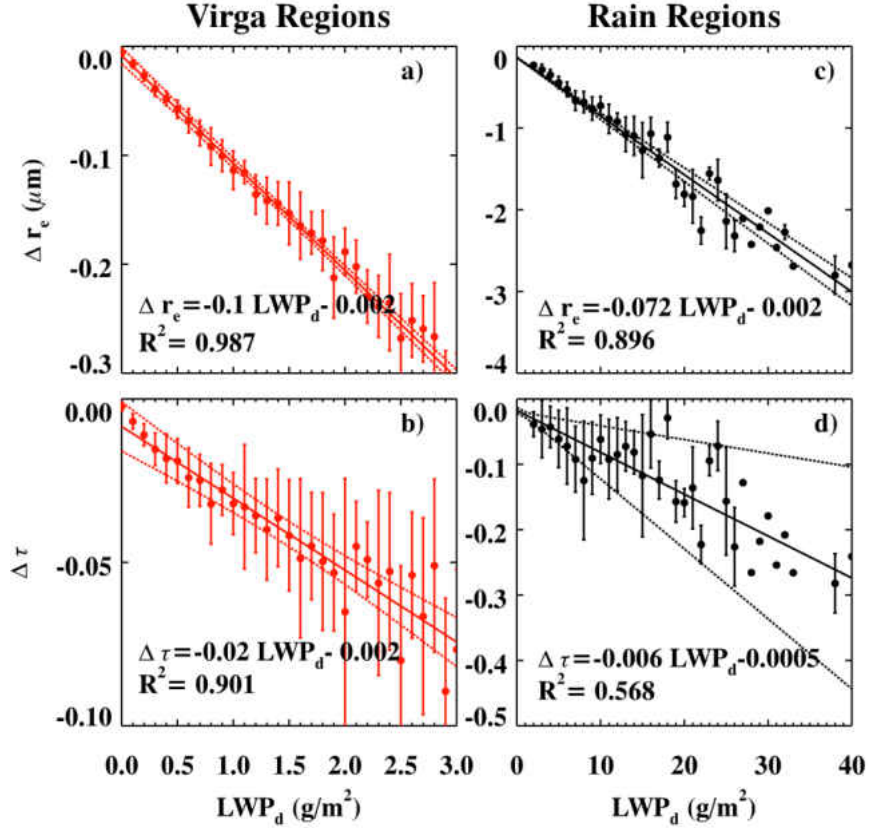
Figure 18. The impact of drizzle on cloud property retrievals (daytime only). Left panel is for the selected virga samples (red line) and right panel is for the selected rain samples (black line). Solid dots denote the mean values of each bin, and the bottom and top of each whisker represent one standard deviation. The solid lines are fitted linear regression lines, the dashed lines indicate upper and lower boundaries of a 95% confidence interval for the regression. Δr_e and $\Delta \tau$ represent the differences between the originally and newly retrieved values.

The sample numbers and seasonal means of retrieved cloud and drizzle microphysical properties for the virga and rain periods are listed in Table 6 and Table 7. A total of 1091 hours (13,090 samples at 5-min resolution, including 4237 virga samples and 1345 rain samples) daytime single-layered MBL clouds has selected from 19-month period (D14a). For the cloud and drizzle samples, the overall drizzle occurrence is 42.6% with a maximum of 55.8% in winter and a minimum of 35.6% in summer. For the virga samples, the seasonal mean LWP_d values (winter to autumn) are 1.87 g m^{-2}, 1.23 g m^{-2},

0.90 g m^{-2}, and 1.16 g m^{-2}, and their corresponding r_d (N_d) values are 42.27 μm (0.36

cm^{-3}), 40.67 μm (0.35 cm^{-3}), 37.25 μm (0.48 cm^{-3}), and 37.68 μm (0.32 cm^{-3}). For the

rain samples, the seasonal mean LWP_d values are 6.83 g m^{-2}, 4.93 g m^{-2}, 4.98 g m^{-2}, and

5.19 g m^{-2}, and their corresponding r_d (N_d) values are 71.08 μm (0.14 cm^{-3}), 71.97 μm

(0.09 cm^{-3}), 63.88 μm (0.21 cm^{-3}), and 67.74 μm (0.13 cm^{-3}). The annual means of LWP_d,

r_d and N_d for the rain (virga) samples are 5.48 g m^{-2} (1.29 g m^{-2}), 68.7 μm (39.5 μm), and

0.14 cm^{-3} (0.38 cm^{-3}). For both virga and rain samples, their LWP_d and r_d are largest

during winter because the dominant low pressure systems and moist air masses during

winter result in more deep frontal clouds associated with midlatitude cyclones, which will

make the MBL clouds deeper and thicker (D14a). On the other hand, their N_d values are

highest but their LWP_d and r_d are minima during summer due to the persistent high

pressure and dry conditions over the Azores (D14a).

Table 6. Seasonal means of drizzle and cloud properties for virga.

	Winter	Spring	Summer	Autumn
Samples (5-min)	464	693	1742	1338
LWP (g m^{-2})	90.48	135.86	108.36	94.84
r_e *(μm)*	12.13	12.94	12.93	11.77
N_t *(cm^{-3})*	76.66	75.98	72.20	90.98
τ	11.70	16.55	13.24	12.67
LWP_d *(g m^{-2})* (% of LWP_d / LWP)	1.87 (2.06)	1.23 (0.91)	0.90 (0.83)	1.16 (1.22)
r_d *(μm)*	42.27	40.67	37.25	37.68
N_d *(cm^{-3})*	0.36	0.35	0.48	0.32
LWP_c *(g m^{-2})*	88.61	134.63	107.46	93.68
r_e' *(μm)*	11.92	12.83	12.84	11.65
N_t' *(cm^{-3})*	78.41	76.75	72.93	91.98
τ'	11.63	16.53	13.22	12.64

Table 7. Seasonal means of drizzle and cloud properties for rain.

	Winter	Spring	Summer	Autumn
Samples (5-min)	244	225	574	302
LWP (g m^{-2})	197.13	269.35	231.41	195.08
r_e (μm)	15.55	16.54	16.41	16.11
N_t (cm^{-3})	30.23	35.85	36.68	35.01
τ	19.41	27.07	22.62	18.89
LWP_d (g m^{-2}) (% of LWP_d / LWP)	6.83 (3.46)	4.93 (1.83)	4.98 (2.15)	5.19 (2.66)
r_d (μm)	71.08	71.97	63.88	67.74
N_d (cm^{-3})	0.14	0.09	0.21	0.13
LWP_c (g m^{-2})	190.30	264.42	226.43	189.89
$r_e{}'$ (μm)	15.08	16.16	16.09	15.68
$N_t{}'$ (cm^{-3})	32.62	37.18	37.84	36.54
τ'	19.31	27.03	22.59	18.83

To investigate seasonal variations of the impact of drizzle on cloud property retrievals, we also calculate the ratio of LWP_d to LWP and cloud properties (r_e, N_t, τ) using (1) with the MWR-retrieved LWP and newly calculated cloud LWP_c (=LWP – LWP_d). Although the annual mean LWP_d from the rain samples is about four times as large as that from the virga samples, their seasonal means are less than 4% of the MWR-retrieved LWP. Therefore, their impact on cloud property retrievals is insignificant. As listed in Table 6 and Table 7, the seasonal differences $(r_e$-$r_e{}')$ are 0.21 (0.47) μm, 0.11 (0.38) μm, 0.09 (0.32) μm, and 0.12 (0.43) μm for the virga (rain) samples with annual mean differences of 0.12 and 0.38 μm, respectively. These differences fall within the cloud property retrieval uncertainty (~10%), validated by in situ aircraft measurements at midlatitude continental sites (Dong et al., 1997, D98, and 2002; DM03). Therefore, the impact of drizzle on cloud-droplet effective radius, in general, can be negligible. However, for some individual cases, the differences can reach as large as 2~3 μm, which

may cause a large uncertainty especially in the study of cloud radiative properties using radiative transfer models (D98). The impacts of drizzle on cloud-droplet number concentration (and optical depth) are also small, presumably due to small changes in both LWP_c and r_e. The annual differences in cloud-droplet number concentration are -0.93 and -1.50 cm^{-3}, respectively, for the virga and rain samples.

CHAPTER IV

CONCLUSIONS AND FUTURE WORK

Summaries and Conclusions

In this study, a method was developed to retrieve nighttime cloud properties over the Azores. Both cloud macro- and micro-physical properties were then investigated in coupled and decoupled boundary layer conditions. Finally, drizzle properties below cloud base were retrieved and the impact of drizzle to cloud property retrievals was quantitatively estimated. The findings from this study are summarized as follows:

1) The new fitted re-dBZ relationship can present MBL cloud microphysical properties for both daytime and nighttime. The nighttime monthly means of r_e are nearly identical to the daytime means with an annual difference of 0.4 μm. The day-night differences in monthly mean N_t and N_{CCN} are very small and their daytime and nighttime PDFs and CDFs are almost the same. The nighttime monthly means of LWP are 30.9 gm^{-2} (28.2%) larger than the daytime means, which results in higher nighttime cloud LWC in most months and optical depth. The PDFs and CDFs of the daytime and nighttime τ values are also very close to each other, and very similar to the PDF and CDF of $LWPs$.

2) Similar to their monthly mean comparisons, the diurnal variation of r_e is small, while the hourly means of LWC and τ basically follow the diurnal variation of LWP: larger nighttime LWP (140 gm^{-2}) than during the daytime (109 gm^{-2}) with semi-diurnal cycle maxima at 0500 LT and 2100 LT, respectively. A semidiurnal

cycle was found in N_{CCN}, there is an increase in surface CCN from around sunrise (0300-0600 LT) to late afternoon, which correlates with surface wind speed (r=0.76) from 0300 to 1900 LT. Hourly means of N_t follow N_{CCN} variations well from midnight to 0900 LT, but not for afternoon and evening with an averaged ratio (N_t / N_{CCN}) of 0.35.

3) Out of a total of 9888 samples, 2196 samples (22.2%) were classified as coupled and 7692 (77.8%) as decoupled; 3234 (32.7%) as non-drizzling and 6654 (67.3%) as drizzling (4726 as virga and 1928 as rain); 4015 (40.6%) as daytime and 5873 (59.4%) as nighttime. The decoupled samples have a higher frequency (68%) of drizzling events compared to the coupled samples (58%). Drizzling events are dominant for both daytime (59%) and nighttime (67%) samples from 19-month samples in this study.

4) The cloud layer depths under non-drizzle and virga are close to each other, but more than 100 m shallower than those of rain, primarily due to lowest Z_b in rain. The averages of coupled and decoupled LWP and r_e values under non-drizzle condition are slightly less than their corresponding averages of virga, but significantly less than the averages of rain. In contrast to LWP and r_e comparisons, the averages of coupled and decoupled N_t under non-drizzle condition are slightly higher than the averages of virga, but ~3-4 times as high as the averages of rain. These results have indicated that the MBL cloud microphysical properties under non-drizzle and virga conditions are similar to each other, but significantly different to those of rain.

5) For the cloud and drizzle samples, the overall drizzle occurrence is 42.6% with a maximum of 55.8% in winter and a minimum of 35.6% in summer. By checking the LWP and N_t values for the four seasons (Table 2), although not necessarily for daytime, it is found that the nighttime LWP in winter is nearly the highest, and more nighttime samples were selected than daytime in the statistics, so the nighttime values should dominate the diurnal mean. The N_t values for both daytime and nighttime are lower in winter than their counterparts in other seasons, so the higher drizzle occurrence in winter might be the combined effect of relatively higher LWP and lower N_t values than other seasons. The annual means of LWP_d, r_d, and N_d for the rain (virga) samples are 5.48 (1.29) g m^{-2}, 68.7 (39.5) μm, and 0.14 (0.38) cm^{-3}, respectively. For both virga and rain samples, their LWP_d and r_d are the largest during winter, whereas their N_d values are at a maximum while their LWP_d and r_d are at a minimum during summer due to different seasonal synoptic patterns.

6) To investigate the impact of drizzle on cloud property retrievals, we calculate the ratio of LWP_d to LWP and cloud properties (r_e, N_t, τ) with the MWR-retrieved LWP and newly calculated cloud LWP_c ($=LWP - LWP_d$). The seasonal mean LWP_d are less than 4% of LWP values. The annual mean differences (r_e-$r_e{'}$) are 0.12 and 0.38 μm, respectively, for the virga and rain samples. These differences fall within the cloud property retrieval uncertainty (~10%). The impacts of drizzle on cloud-droplet number concentration (optical depth) are also small, presumably due to small changes in both LWP_c and r_e. Therefore, we can conclude that the impact of drizzle on cloud property retrievals is insignificant.

Future Work

Retrieval of Drizzle Properties in the Cloud

Drizzle particles are produced near cloud top and then fall to cloud base, growing larger in this process. Drizzle depletes water and CCN from clouds, so drizzle within the clouds act as the "source" of both virga and rain, ultimately affecting thermodynamics and cloud evolution in the MBL (Stevens et al. 1998). Wood (2005a) proposed that drizzle and CCN may be important in driving the transition from a deep, near-frontal cloud layer to a shallow subsidence-dominated MBL. Recent studies (Wood 2005a, Geoffroy et al. 2008, Wood 2012) have found that aerosols may play an important role in controlling MBL precipitation and the precipitation rate decreases with the increase of cloud droplet number concentration for a given amount of condensate or cloud thickness. Study in this thesis only focus on drizzle below cloud base, to further understand the effects of drizzle on cloud life cycle and sub-cloud dynamics, the properties of drizzle within the cloud need to be retrieved. However, when drizzle is present in the cloud layer, radar reflectivity is dominated by several large drizzle particles, which makes it difficult to retrieve cloud and drizzle properties from radar reflectivity directly. To overcome this problem, we will develop a method to retrieve drizzle properties within the cloud using an adiabatic method.

An adiabatic method is under developing to retrieve adiabatic *LWC* and cloud droplet radius profiles using radiosonde soundings. Atmospheric pressure, temperature, and relative humidity profiles measured by radiosonde soundings are used to calculate the adiabatic liquid water mixing ratio and air mass density. The adiabatic *LWC* profile is calculated based on the moist adiabatic assumption, where adiabatic *LWC* is the product of adiabatic liquid water mixing ratio and air mass density.

If a saturated parcel moves vertically an amount $\Delta Z = Z_{i+1} - Z_i$ on a moist adiabatic and

retains the condensed liquid water, then its increase in liquid water content is

$$\Delta\, LWC_{ad}(\Delta Z = Z_{i+1} - Z_i) \approx \frac{C_p \overline{\rho_{i+1,i}}}{2}\left[\frac{\Gamma_d - \Gamma_s(z_{i+1})}{L(z_{i+1})} + \frac{\Gamma_d - \Gamma_s(z_i)}{L(z_i)}\right]\Delta Z, \tag{17}$$

where

$$\overline{\rho_{i+1,i}} = \frac{1}{2}\left(\rho_{air}(z_{i+1}) + \rho_{air}(z_i)\right). \tag{18}$$

ρ_{air} is the density of dry air, $C_p = 1004\, J\, K^{-1} kg^{-1}$ is the specific heat of dry air at

constant pressure, $\Gamma_d = 9.8$ °K km^{-1} is the dry adiabatic lapse rate, $L(z_i)$ is the latent heat

of vaporization at z_i, and $\Gamma_s(z_i)$ is the moist adiabatic lapse rate at z_i. Therefore,

$$LWC_{ad}(z_{i+1}) = LWC_{ad}(z_i) + \Delta LWC_{ad}(z_{i+1} - z_i). \tag{19}$$

At each level, $L(z_i)$ and $\Gamma_s(z_i)$ are calculated from the radiosonde measured pressure,

temperature and relative humidity profiles, and $LWC_{ad}(z_{i+1})$ is computed from (19).

The adiabatic LWC, in general, is larger than the observed LWC due to entrainment at

cloud top (Slingo 1982). A variable, f_{ad}, was introduced (Wood 2005a) to represent the

overall adiabaticity of vertically integrated liquid water with

$$f_{ad} = LWP/LWP_{ad}. \tag{20}$$

where LWP is from MWR, LWP_{ad} is integrated from adiabatic LWC. Wood (2005)

provided the vertical profile of LWP/LWP_{ad} using data from 12 flights (Fig. 20). Here,

we adapt a "standard adiabaticity profile" from Wood (2005a) if we assume the clouds in

Wood (2005a) can represent general properties of MBL clouds, the profile of adiabaticity

is shown in Fig. 21. The actual LWC estimated using adiabatic method will then be

computed using

$$LWC(z_i) = LWC_{ad}(z_i) * f_{ad}(z_i). \tag{21}$$
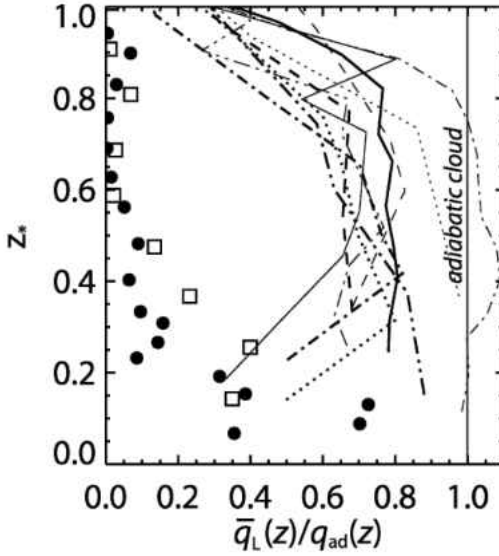
Figure 19. Profiles of adiabaticity from Wood (2005a). (For different symbols, please refer to Wood 2005a)
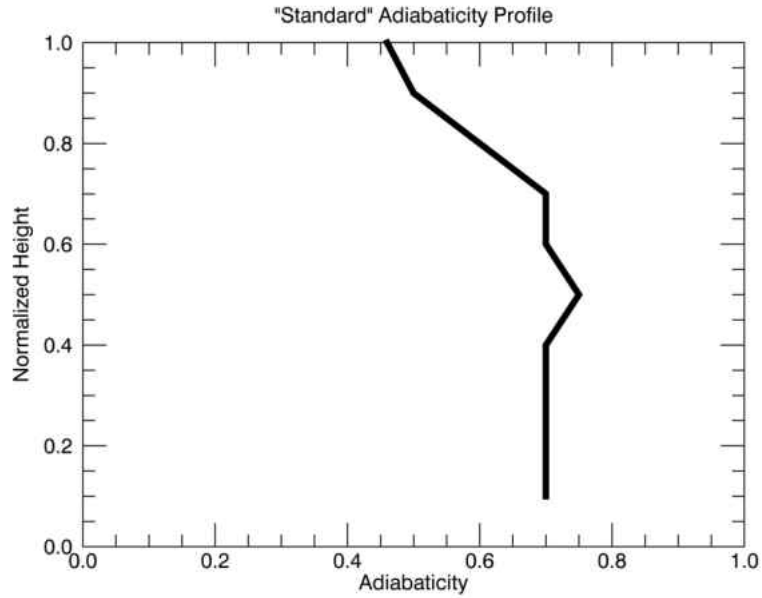

Figure 20. A standard profile of adiabaticity adapted from Wood (2005a). Cloud height is normalized from bottom (0) to cloud top (1).

The vertical profile of cloud droplet effective radius, according to DM03, can be estimated by

$$r_e(z) = \left[\frac{3LWC(z)}{4\pi N \rho_w \exp(4.5\sigma_x^2)}\right]^{1/3} \exp(2.5\sigma_x^2). \tag{22}$$

Here, σ_x is logarithmic width and is set to 0.38 (Miles et al. 2000), N is cloud droplet number concentration and use the values from Dong et al. (1998, hereafter D98), ρ_w is water density. The profile of r_e is further constrained by the result from D98: after r_e profile was computed, the layer mean value was calculated. The ratio of this layer mean value and D98 was then used to regulate the calculated r_e profile, such that the new calculated layer mean is equal to that from D98.

The cloud LWP (LWP_c) can be computed by integrating cloud LWC which can be calculated from:

$$LWC_c = \frac{4\pi}{3}\rho_w N r_e^3 \exp(4.5\sigma_x^2). \qquad (23)$$

Drizzle LWP (LWP_d) can then be calculated by subtracting LWP_c from MWR retrieved LWP. The cloud reflectivity factor, according to DM03, can then been calculated as

$$Z_{ad} = 2^6 10^{-12} N r_e^6 \exp(3\sigma_x^2), \qquad (24)$$

The reflectivity factor generated by drizzle particles in the cloud can be calculated by subtracting the cloud reflectivity factor from WACR measured reflectivity:

$$Z_{drizzle} = Z_{WACR} - Z_{ad}. \qquad (25)$$

Figure 22 shows the reflectivity for drizzle in the cloud (Fig. 22c). The majority of the reflectivity appears near cloud base; this is reasonable since drizzle particles tend to grow larger through collision/coalescence and accretion while it falls from cloud top all the way down to the cloud base. The reflectivity of drizzle in and below cloud base are continuous as shown in Fig. 22d,indicating that this method might be a solution to get drizzle properties inside clouds. However, as discussed above, drizzle form near the cloud top, where almost no reflectivity was calculated using the adiabatic method,

63

because the drizzle particles are relatively small. Entrainment at the cloud top might be one of the reasons. Also, information is insufficient to retrieve drizzle property profiles only with the information of LWP_d and reflectivity, thus further information is needed. Future work will be performed to address this part.
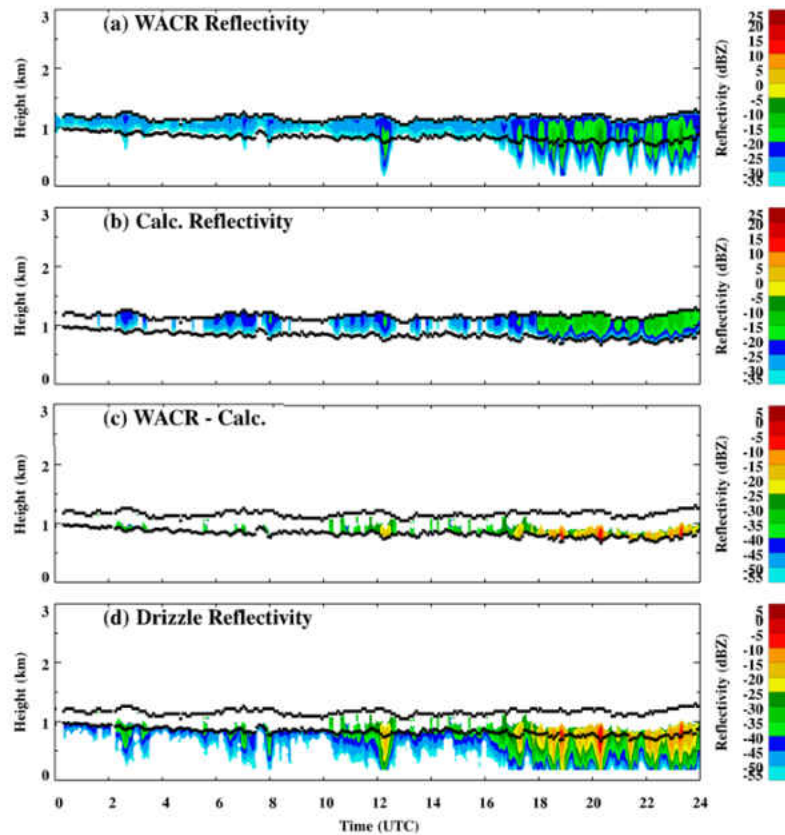
Figure 21. Reflectivity of (a) WACR observed, (b) calculated using adiabatic method, (c) difference of observed and calculated, and (d) drizzle in and below cloud base for Nov. 08, 2010 over the Azores. Black dots indicate cloud base and top heights. Note that different colorbars were used in panels (a), (b) and panels (c), (d).

A larger uncertainty for this approach rise from the adiabaticity profile adapted from Wood (2005a), the turnover of the profiles in Wood (2005a) were mainly due to horizontal averaging of aircraft legs that go in and out of cloud top, so the cloud properties profiles calculated using the adapted adiabaticity profile will have larger uncertainties near the cloud top than for the lower part of cloud.

Another possible way to retrieve cloud properties is to calculate cloud radiative properties first, since, according to D98, drizzle has little effect on solar transmission, so the measured shortwave flux is little affected by drizzle particles in the cloud. D98 can only get the layer mean information of cloud properties, so it will be hard drizzle information from observed radar reflectivity profiles. The cloud radiative properties such extinction efficiency can provide another profile of cloud in addition to reflectivity, Doppler velocity and spectral width.

The recent deployed permanent fixed ARM site (Eastern North Atlantic (ENA) Site) at the Azores started in late 2013 (Wood et al. 2015) will provide long term observations and more comprehensive MBL cloud information to date. The high quality data provide the possibility of performing our future work.

REFERENCES

American Meteorological Society, 2015: virga, *Glossary of Meteorology.* Available at http://glossary.ametsoc.org/wiki/Virga/, last access: 6 March, 2015.

Albrecht, B.A., 1993: The effects of drizzle on the thermodynamic structure of the trade-wind boundary layer*, J. Geophys. Res., 98*, 7327-7337.

Albrecht, B. A., C. S. Bretherton, D. Johnson, W. H. Schubert, and A. S. Frisch, 1995: The Atlantic Stratocumulus Transition Experiment—ASTEX. *Bull. Amer. Meteor. Soc.*, 76, 889–904.

Austin, P., Y. Wang, R. Pincus, and V. Kujala, 1995: Precipitation in stratocumulus clouds: Observations and modeling results, *J. Atmos. Sci., 52*, 2329–2352.

Bony, S., and J.-L. Dufresne, 2005: Marine boundary layer clouds at the heart of cloud feedback uncertainties in climate models. *Geophys. Res. Lett*., 32, L20806, doi:10.1029/2005GL023851.

Bretherton, C. S., T. Uttal, C. W. Fairall, S. E. Yuter, R. A. Weller, D. Baumgardner, K. Comstock, and R. Wood, 2004: The EPIC 2001 stratocumulus study. *Bull. Amer. Meteor. Soc.*, 85, 967–977.

Burleyson, C. D., S. P. de Szoeke, S. E. Yuter, M. Wilbanks, and W. A. Brewer, 2013: Ship-based observations of the diurnal cycle of southeast Pacific marine stratocumulus clouds and precipitation, *J. Atmos. Sci.*, 70, 3876-3894, doi:10.1175/JAS-D-13-01.1.

Caldwell, P., C. S. Bretherton, and R. Wood, 2005: Mixed-Layer Budget Analysis of the Diurnal Cycle of Entrainment in Southeast Pacific Stratocumulus. J. Atmos. Sci., 62, 3775–3791.

Cess, R. D., and Coauthors, 1990: Intercomparison and interpretation of climate feedback processes in 19 atmospheric general circulation models. *J. Geophys. Res*., 95, 16 601-16 615.

Cess, R. D., and Coauthors, 1996: Cloud feedback in atmospheric general circulation models: An update. *J. Geophys. Res*., 101, 12 791–12 794.

Chen, T., W. B. Rossow, and Y. C. Zhang, 2000: Radiative effects of cloud-type variations. *J. Clim*, 13, 264–286.

Chin, H., and coauthors, 2000: A microphysical retrieval scheme for continental low-level stratiform clouds: Impacts of the subadiabatic character on microphysical properties and radiation budgets, *Mon. Weather Rev., 128*, 2511 – 2527.

Dolinar, E., X. Dong, and B. Xi, 2015: Evaluation and Intercomparison of Clouds, Precipitation, and Radiation Budgets in Recent Reanalyses using Satellite-Surface Observations. Climate Dynamics, DOI: 10.1007/s00382-015-2693-z.

Dong X., T.P. Ackerman, E.E. Clothiaux, Pilewskie, and Y. han, 1997: Microphysical and Radiative Properties of Stratiform Clouds Deduced from Ground-based Measurements. *J. Geophys. Res*., 102, 23829-23843.

Dong, X., T. P. Ackerman, and E. E. Clothiaux, 1998: Parameterizations of microphysical and Shortwave radiative properties of boundary layer stratus from ground-based measurements. *J. Geophys. Res*., 102, 31,681-31,393.

Dong, X., P. Minnis, T. P. Ackerman, E. E. Clothiaux, G. G. Mace, C. N. Long, and J. C. Liljegren, 2000: A 25-month database of stratus cloud properties generated from ground-based measurements at the ARM SGP site. *J. Geophys. Res*., 105, 4529-4538.

Dong X. , P. Minnis, G.G. Mace, W.L. Smith Jr, M. Poellt, R. Marchand, and Anita D. Rapp, 2002: Comparison of stratus cloud properties deduced from surface, GOES, and aircraft data during the March 2000 ARM Cloud IOP. *J. Atmos. Sci*., 59, 3265-3284.

Dong X. and G.G. Mace, 2003: Profiles of Low-level Stratus Cloud Microphysics Deduced from Ground-based Measurements. *J. Atmos and Oceanic Tech*., 20, 42-53.

Dong X., P. Minnis, and B. Xi, 2005: A climatology of midlatitude stratus clouds from ARM SGP site: Part I:Macrophysical, microphysical and radiative properties. *J. Clim.,* 18 , 1391-1410.

Dong, X., B. Xi, A. Kennedy, P. Minnis and R. Wood, 2014a: A 19-month Marine Aerosol-Cloud-Radiation Properties derived from DOE ARM AMF deployment at the Azores: Part I: Cloud Fraction and Single-layered MBL cloud Properties, *J. Clim., 27*, doi:10.1175/JCLI-D-13-00553.1

Dong, X., B. Xi, and P. Wu, 2014b: Investigation of Diurnal Variation of MBL Cloud Microphysical Properties at the Azores, *J. Clim., 27*, 8827-8835

Dong, X., A. Schwantes, B. Xi and P. Wu, 2015: Investigation of the Marine Boundary Layer Cloud Properties under Coupled and Decoupled Conditions at the Azores. *J. Geophys. Res. Atmos.,* 120, doi:10.1002/2014JD022939.

67

Fox, Neil I., and Anthony J. Illingworth, 1997: The Potential of a Spaceborne Cloud Radar for the Detection of Stratocumulus Clouds. *J. Appl. Meteor.*, 36, 676–687.

Fielding, M. D., J. C. Chiu, R. J. Hogan, G. Feingold, E. Eloranta, E. J. O'Connor, and M. P. Cadeddu, 2015: Joint retrievals of cloud and drizzle in marine boundary layer clouds using ground-based radar, lidar and zenith radiances. *Atmos. Meas. Tech. Discuss.*, 8, 1833–1889, 2015.

Frisch, A. S., C. W. Fairall, and J. B. Snider, 1995: Measurement of stratus cloud and drizzle parameters in ASTEX with a Ka-band Doppler radar and a microwave radiometer, *J. Atmos. Sci., 52*, 2788–2799.

Geoffroy, O., Brenguier, J.-L., and Sandu, I., 2008: Relationship between drizzle rate, liquid water path and droplet concentration at the scale of a stratocumulus cloud system, *Atmos. Chem. Phys.*, 8, 4641-4654, doi:10.5194/acp-8-4641-2008.

Hahn, C. J., and S. G. Warren, 2007: A gridded climatology of clouds over land (1971–96) and ocean (1954–97) from surface observations worldwide. Numeric Data Package NDP-026EORNL/CDIAC-153, CDIAC, Department of Energy, Oak Ridge, TN.

Hartmann, D. L., M. E. Ockert-Bell, and M. L. Michelsen, 1992: The effect of cloud type on earth's energy balance—Global analysis. *J. Clim.*, 5, 1281–1304.

Holdridge, D., and coauthors, 2011: Balloon-Borne Sounding System (SONDE) Handbook. DOE/SC-ARM/TR-029, Department of Energy.

Jones, C., C. Bretherton, and D. Leon, 2011: Coupled vs. decoupled boundary layers in VOCALS-Rex, *Atmos. Chem. Phys.*, 11, 7143-7153.

Klein, S. A., and D. L. Hartmann, 1993: The seasonal cycle of low stratiform clouds. *J. Clim.*, 6, 1588–1606.

Kubar, T. L., D. L. Hartmann, and R. Wood, 2009: Understanding the importance of microphysics and macrophysics for warm rain in marine low clouds. Part I: Satellite observations, *J. Atmos. Sci.*, 66(10), 2953–2972, doi:10.1175/2009JAS3071.1.

Leon, D. C., Z. Wang, and D. Liu, 2008: Climatology of drizzle in marine boundary layer clouds based on 1 year of data from CloudSat and Cloud-Aerosol Lidar and Infrared Pathfinder Satellite Observations (CALIPSO), *J. Geophys. Res., 113*, D00A14, doi:10.1029/2008JD009835.

Liljegren J. C., 2001: A new retrieval for cloud liquid water path using a ground-based microwave radiometer and measurements of cloud temperature. *J. Geophys. Res. Atmos.*, 106, 14485-14500.

Lilly, D. K, 1968: Models of cloud-topped mixed layers under a strong inversion. *Quart. J. Roy. Meteor. Soc.,* 94, 292-309.

Logan, T., B. Xi, and X. Dong, 2014: Aerosol Physical and Chemical Properties and Their Interaction with CCN over the AMF-Azores Facility. *J. Geophys. Res.*, 119, doi:10.1002/2013JD021288.

Lu, M.-L., W. C. Conant, H. H. Jonsson, V. Varutbangkul, R. C. Flagan, and J. H. Seinfeld, 2007: The Marine Stratus/Stratocumulus Experiment (MASE): Aerosol-cloud relationships in marine stratocumulus, *J. Geophys. Res.,* 112, D10209.

Mace, G. G., and K. Sassen, 2000: A constrained algorithm for retrieval of stratocumulus cloud properties using solar radiation, microwave radio- meter, and millimeter cloud radar data, *J. Geophys. Res., 105*, 29,099–29,108.

Miles, N.L., J. Verlinde, and E.E. Clothiaux, 2000: Cloud-droplet size distributions in low-level stratiform clouds. *J. Atmos. Sci.,* **57**, 295-311.

Morris, V. R., 2006: Microwave Radiometer (MWR) Handbook. ARM TR-016, Department of Energy.

Nicholls, S., 1984: The dynamics of stratocumulus: Aircraft observations and comparisons with a mixed layer model. *Quart. J. Roy. Meteor. Soc.*, 110, 783–820.

O'Connor, E. J., R. J., Hogan, and A. J., Illingworth, 2005: Retrieving stratocumulus drizzle parameters using Doppler radar and lidar, *J. of Applied Meteorol.,* 44, 14-27.

Kollias, P., E. E. Clothiaux, M. A. Miller, E. P. Luke, K. L. Johnson, K. P. Moran, K. B. Widener, and B. A. Albrecht, 2007: The Atmospheric Radiation Measurement Program cloud profiling radars: Second-generation sampling strategies, processing, and cloud data products. *J. Atmos. Oceanic Technol.*, 24, 1199–1214.

Ramanathan, V. L. R. D., Cess, R. D., Harrison, E. F., Minnis, P., Barkstrom, B. R., Ahmad, E., & Hartmann, D., 1989: Cloud-radiative forcing and climate: Results from the Earth Radiation Budget Experiment. *Science*, 243(4887), 57-63.

Randall, D. A., 1984: Stratocumulus cloud deepening through entrainment. *Tellus*, 36A, 446–457.

Rémillard, J., P. Kollias, E. Luke, and R. Wood, 2012: Marine Boundary Layer Cloud Observations in the Azores, *J. Clim.,* 25 (21), 7381–7398

Rogers, R. R., and M. K., Yau, 1989: A short course in cloud physics, 3rd ed., 125-126, *Peramon press*, New York, USA.

Rozendaal, M. A., C. B. Leovy, and S. A. Klein, 1995: An observational study of the diurnal cycle of marine stratiform cloud. *J. Clim.*, 8, 1795–1809.

Shin, Sun-Hee, and Kyung-Ja HA, 2009: Implementation of Turbulent Mixing over a Stratocumulus-Topped Boundary Layer and Its Impact in a GCM, *Advances in Atmos. Sci.,* 26, 1–10.

Slingo, A., and Schrecker, H. M., 1982: On the shortwave radiative properties of stratiform water clouds. *Quart. J. Roy. Meteor. Soc.*, 108(456), 407-426.

Slingo, A., 1990: Sensitivity of the earth's radiation budget to changes in low clouds. *Nature*, 343, 49-51.

Sauvageot, H., and J. Omar, 1987: Radar reflectivity of cumulus clouds, *J. Atmos. Oceanic Technol., 4*, 264–272.

Serpetzoglou, E., B. A. Albrecht, P. Kollias, and C. W. Fairall, 2008: Boundary layer, cloud, and drizzle variability in the southeast Pacific stratocumulus regime. *J. Clim.*, 21, 6191–6214.

Schwantes, A. C, 2014: Investigation of Stratocumulus Micro and Macro-physical Properties under Coupled and Decoupled Boundary Layer regimes Over the ARM Azores Site, M.S. thesis, Dep. of Atmos. Sci., Univ. of North Dakota, Grand Forks, ND, USA.

Soden, B. J., and G. A. Vecchi, 2011: The vertical distribution of cloud feedback in coupled ocean-atmosphere models. *Geophys. Res. Lett.*, 38, L12704, doi: 10.1029/2011GL047632

Stephens, G. L., and T. J. Greenwald, 1991: Observations of the Earth's radiation budget in relation to atmospheric hydrology. Part II: Cloud effects and cloud feedback. *J. Geophys. Res.,* 96, 15 325–15 340.

Stevens, B., W. R. Cotton, G. Feingold, and C.-H. Moeng, 1998: Large-eddy simulations of strongly precipitating, shallow, stratocumulus-topped boundary layers. *J. Atmos. Sci.*, 55, 3616–3638.

Stevens, B., and Coauthors, 2003: Dynamics and Chemistry of Marine Stratocumulus—DYCOMS II. *Bull. Amer. Meteor. Soc.*, 84, 579–593.

Troyan, D., 2012: Merged Sounding Value-Added Product. DOE/SC-ARM/TR-087, Department of Energy.

Wang, J., 2002: Identifying Drizzle within Marine Stratus with W-Band Radar Reflectivity profiles, M.S. thesis, Dep. Of Atmos. Sci., Univ. of Wyoming, Laramie, USA.

Wang, J., and B. Geerts, 2003: Identifying drizzle within marine stratus with W-band radar reflectivity. *Atmos. Res., 69*, 1–27.

Warren, S. G., C. J. Hahn, J. London, R. M. Chervin, and R. L. Jenne, 1986: Global distribution of total cloud cover and cloud types over land. NCAR Tech. Note NCAR/TN-2731STR, National Center for Atmospheric Research, Boulder, CO, 29 pp. 1 200 maps.

Warren, S. G., C. J. Hahn, J. London, R. M. Chervin, and R. L. Jenne, 1988: Global distribution of total cloud cover and cloud types over ocean. NCAR Tech. Note NCAR/TN-3171STR, National Center for Atmospheric Research, Boulder, CO, 42 pp. 1 170 maps.

Wood, R., 2000: Parameterization of the effect of drizzle upon the droplet effective radius in stratocumulus clouds. *Q.J.R. Meteorol. Soc., 126*: 3309–3324. doi: 10.1002/qj.49712657015

Wood, R., C. S. Bretherton, and D. L. Hartmann, 2002: Diurnal cycle of liquid water path over the subtropical and tropical oceans. *Geophys. Res. Lett*., 29, 2092, doi:10.1029/2002GL015371.

Wood, R., and C. S. Bretherton, 2004: Boundary layer depth, entrainment, and decoupling in the cloud-capped subtropical and tropical marine boundary layer. *J. Clim.*, 17, 3576–3588.

Wood, R., 2005a: Drizzle in Stratiform Boundary Layer Clouds. Part I: Vertical and Horizontal Structure. *J. Atmos. Sci*., 62, 3011-3033.

Wood, R., 2005b: Drizzle in Stratiform Boundary Layer Clouds. Part II: Microphysical Aspects, *J. Atmos. Sci*., 62, 3034-3050.

Wood, R., and D. L. Hartmann, 2006: Spatial variability of liquid water path in marine boundary layer clouds: The importance of mesoscale cellular convection. *J. Clim*., 19, 1748–1764.

Wood, R., T. Kubar, and D. L. Hartmann, 2009: Understanding the importance of microphysics and macrophysics for warm rain in marine low clouds: Part II. Heuristic models of rain formation. *J. Atmos. Sci*., 66, 2973-2990.

Wood, R., and Coauthors, 2011: The VAMOS Ocean-Cloud-Atmosphere-Land Study Regional Experiment (VOCALS-REx): Goals, platforms, and field operations. *Atmos. Chem. Phys*., 11, 627–654.

Wood, R., 2012: Review: stratocumulus clouds. *Mon. Wea. Rev*., 140, 2373-2423.

Wood, R., and coauthors, 2015: Clouds, Aerosol, and Precipitation in the Marine Boundary Layer: An ARM Mobile Facility Deployment. *Bull. Amer. Meteor. Soc*., DOI:10.1175/BAMS-D-13-00180.1

Xi, B., X. Dong, P. Minnis, and S. Sun-Mack, 2014: Validation of CERES-MODIS Edition 4 Marine Boundary Layer Cloud Properties using DOE ARM AMF Measurements and the AZORES. *J. Geophys. Res*., 119, doi: 10.1002/2014JD021813.

Zhao, C., and coauthors, 2012: Toward understanding of differences in current cloud retrievals of ARM ground-based measurements. *J. Geophys. Res., 117,* D10206, doi:10.1029/2011JD016792.

Zuidema, P., and D. L. Hartmann, 1995: Satellite determination of stratus cloud microphysical properties. *J. Clim*., 8, 1638–1656.

Zuidema, P., E. R. Westwater, C. Fairall, and D. Hazen, 2005: Ship-based liquid water path estimates in marine stratocumulus. *J. Geophys. Res*., 110, D20206, doi: 10.1029/2005JD005833.

Jefferson, A., 2011: Aerosol Observing System (AOS) Handbook. ARM-TR-014, Department of Energy.